2013

Functional analysis of a migraine-associated TRESK K+ channel mutation

Ping Liu
Washington University School of Medicine in St. Louis

Zheman Xiao
Washington University School of Medicine in St. Louis

Fei Ren
Washington University School of Medicine in St. Louis

Zhaohua Guo
Washington University School of Medicine in St. Louis

Ziwei Chen
Washington University School of Medicine in St. Louis

See next page for additional authors

Neurobiology of Disease

Functional Analysis of a Migraine-Associated TRESK K^+ Channel Mutation

Ping Liu,[1,2]* Zheman Xiao,[1,2]* Fei Ren,[1,2]* Zhaohua Guo,[1,2] Ziwei Chen,[2] Hucheng Zhao,[1,2] and Yu-Qing Cao[1,2]

[1]Washington University Pain Center and [2]Department of Anesthesiology, Washington University School of Medicine, St. Louis, Missouri 63110

Recent genetic and functional studies suggest that migraine may result from abnormal activities of ion channels and transporters. A frameshift mutation in the human TWIK-related spinal cord K^+ (TRESK) channel has been identified in migraine with aura patients in a large pedigree. In *Xenopus* oocytes, mutant TRESK subunits exert a dominant-negative effect on whole-cell TRESK currents. However, questions remain as to whether and how mutant TRESK subunits affect the membrane properties and the excitability of neurons in the migraine circuit. Here, we investigated the functional consequences of the mutant TRESK subunits in HEK293T cells and mouse trigeminal ganglion (TG) neurons. First, we found that mutant TRESK subunits exhibited dominant-negative effects not only on the size of the whole-cell TRESK currents, but also on the level of TRESK channels on the plasma membrane in HEK293T cells. This likely resulted from the heterodimerization of wild-type and mutant TRESK subunits. Next, we expressed mutant TRESK subunits in cultured TG neurons and observed a significant decrease in the lamotrigine-sensitive K^+ current, suggesting that the mutant TRESK subunits have a dominant-negative effect on currents through the endogenous TRESK channels. Current-clamp recordings showed that neurons expressing mutant TRESK subunits had a higher input resistance, a lower current threshold for action potential initiation, and a higher spike frequency in response to suprathreshold stimuli, indicating that the mutation resulted in hyperexcitability of TG neurons. Our results suggest a possible mechanism through which the TRESK mutation increases the susceptibility of migraine headache.

Introduction

Migraine affects >10% of the general population and often results in debilitating headache, accompanied by other symptoms such as aura (Victor et al., 2010). Multiple mutations of voltage-gated Ca^{2+} and Na^+ channels and the Na^+-K^+ pump have been associated with familial hemiplegic migraine, a rare hereditary migraine (Ophoff et al., 1996; De Fusco et al., 2003; Dichgans et al., 2005). Recently, a dominant-negative mutation in the KCNK18 gene encoding the human TWIK-related spinal cord K^+ (TRESK) channel was linked to migraine with aura in a large pedigree (Lafrenière et al., 2010). Subsequently, more missense TRESK variants have been found in unrelated patients (Lafrenière and Rouleau, 2011; Andres-Enguix et al., 2012; Lafrenière and Rouleau, 2012). The fact that all of these proteins are involved in transporting ions across the plasma membrane suggests that these familial migraines may result from abnormal ionic homeostasis, neuronal excitability, and/or neurotransmission, as in the case of epilepsy, episodic ataxia, and other channelopathies. Many of the symptoms, including headache and aura, are identical in familial and general migraine, suggesting a common pathophysiology. Therefore, research on the functional consequences of these mutations provides an entry point for understanding the mechanisms underlying familial migraine and more general forms of migraine.

TRESK is a Ca^{2+}-activated two-pore domain K^+ (K_{2P}) channel that is abundantly expressed in primary afferent neurons in trigeminal ganglion (TG) and dorsal root ganglion (DRG) (Sano et al., 2003; Kang et al., 2004; Lafrenière et al., 2010). Previous physiological studies indicate that TRESK is one of the major background K^+ channels in DRG neurons and contributes to DRG neuronal excitability in both normal and disease settings (Kang and Kim, 2006; Dobler et al., 2007; Tulleuda et al., 2011; Marsh et al., 2012; Plant, 2012). The identification of multiple frameshift and missense *KCNK18* mutations in migraine patients implicates a role of TRESK channels in migraine pathophysiology (Lafrenière and Rouleau, 2011, 2012). When expressed in *Xenopus* oocytes, mutant subunits exert a dominant-negative effect on whole-cell TRESK currents (Lafrenière et al., 2010; Andres-Enguix et al., 2012), suggesting that the mutant channels may affect the normal function of neurons in the migraine circuit. Several important questions, however, remain to be addressed. For example, does the dominant-negative effect of TRESK muta-

Received March 11, 2013; revised June 28, 2013; accepted June 28, 2013.

Author contributions: P.L., Z.X., F.R., Z.C., and Y.-Q.C. designed research; P.L., Z.X., F.R., Z.G., Z.C., and H.Z. performed research; P.L., Z.X., F.R., Z.G., Z.C., H.Z., and Y.-Q.C. analyzed data; P.L., Z.X., F.R., Z.G., Z.C., and Y.-Q.C. wrote the paper.

This work was supported by the National Institutes of Health–National Institute of Neurological Disorders and Stroke (Grants #R21NS066202 and #R21NS074198 to Y.-Q.C.) and the Xiangya Scholarship Fund (to F.R.). We thank Drs. Robert W. Gereau IV, Christopher Lingle, Joe Henry Steinbach, and Alex Evers for helpful discussions during the preparation of this manuscript, Dr. Daizong Li for helping in the generation of the TRESK antibody, and Joanna Luo for technical assistance.

The authors declare no competing financial interests.

*P.L., Z.X., and F.R. contributed equally to this work.

Correspondence should be addressed Dr. Yu-Qing Cao, Department of Anesthesiology and Pain Center, Washington University School of Medicine, 660 South Euclid, Box 8054, St. Louis, MO 63110. E-mail: caoy@anest.wustl.edu.

Z. Xiao's present address: Department of Neurology, Renmin Hospital, Wuhan University, 238 Jiefang Rd, Wuchang, Wuhan, Hubei, China, 430060.

F. Ren's present address: Department of Anesthesiology, Xiangya Hospital, Central South University, 87 Xiangya Rd, Changsha, Hunan, China, 410008.

DOI: 10.1523/JNEUROSCI.1237-13.2013

 0270-6474/13/3312810-15$15.00/0

tion exist in neurons? Does the expression of mutant TRESK subunits affect neuronal excitability?

Here, we report the first detailed investigation of the functional consequences of a frameshift TRESK mutation in HEK293T cells and TG neurons. We found that the mutant TRESK subunits form nonfunctional channels *per se*. When coexpressed with the wild-type TRESK, mutant subunits exhibited a dominant-negative effect on the whole-cell TRESK currents and the plasma membrane localization of TRESK channels. We show here that expression of mutant TRESK subunits in TG neurons resulted in a decrease of the endogenous TRESK currents, an increase in input resistance (R_{in}), and ultimately an increase in neuronal excitability. (Portions of this manuscript have been published previously in abstract form; Liu et al., 2012).

Materials and Methods

Wild-type and mutant mouse TRESK constructs. The coding region of the mouse TRESK K^+ channel (encoded by the kcnk18 gene) was PCR amplified from a plasmid purchased from Open Biosystems and cloned into the plasmid pIRES2-DsRed-Express2 (Clontech) to generate the construct wtTRESK-IRES-DsRed. Using the Stratagene QuikChange Site-Directed Mutagenesis Kit, we introduced the 2 bp CT deletion identified from a familial migraine with aura pedigree (Lafrenière et al., 2010) into the corresponding region of the mouse TRESK cDNA in wtTRESK-IRES-DsRed construct to generate the mtTRESK-IRES-DsRed construct.

The frameshift mutation results in the premature truncation of human TRESK protein from 384 to 162 aa. The truncated TRESK protein includes the intact cytosolic N terminus, the first transmembrane region, the first extracelluar loop (aa 1–138) and a 24 aa aberrant sequence at the C terminus (Lafrenière et al., 2010). The corresponding mutation has very similar effects on the mouse TRESK, generating a truncated protein with the first 149 aa of wild-type TRESK and a 50 aa aberrant sequence at the C terminus. The EGFP- or mCherry-tagged wild-type and mutant TRESK constructs were generated by fusing wild-type and mutant TRESK cDNAs in-frame at the C termini of EGFP and mCherry coding region (EGFP-WT, mCherry-WT, EGFP-MT, and mCherry-MT, respectively). The V5 and HA epitope-tagged wild-type and mutant TRESK constructs (V5-WT, V5-MT, HA-WT, and HA-MT, respectively) were generated by replacing the EGFP coding region with the V5 and HA coding sequence. All PCR-generated cDNA fragments and linker regions were sequenced completely to verify the mutation and to make sure that no additional mutations were introduced. In all constructs, the TRESK coding regions were inserted downstream of the CMV promoter.

Cell culture, transfection, and image analysis. Human embryonic kidney 293T (HEK293T) cells (ATCC) were maintained in 6-well plates in DMEM with 10% FBS and transfected with Lipofectamine 2000 (Invitrogen). We used wtTRESK-IRES-DsRed and mtTRESK-IRES-DsRed constructs for electrophysiology experiments and the EGFP- or mCherry-tagged TRESK constructs for imaging analysis. One day after transfection, cells were seeded on Matrigel-coated coverslips. Transfected cells were identified by the EGFP, DsRed, or mCherry fluorescence and used for patch-clamp recordings or imaging analysis 2–3 d after transfection.

For each set of experiments, the fluorescence intensity was quantified in cells that underwent a parallel experimental procedure and image analysis process. All conditions were identical, except for the DNA constructs. Fluorescent images were captured through a 40× objective (numerical aperture 1.3) on a Nikon TE2000S inverted epifluorescence microscope equipped with a CoolSnap HQ^2 camera (Photometrics). SimplePCI software (Hamamatsu) was used for image analysis. To measure the expression level of EGFP- or mCherry-tagged TRESK proteins, a single cell was specified as a region of interest (ROI). The intensity of EGFP and/or mCherry signal was determined on a pixel-by-pixel basis and was averaged for each ROI. For each image captured, the mean intensity of the cell-free regions was taken as the background level and was subtracted from the mean intensity in each ROI.

To measure the thickness of the plasma membrane, we incubated live cells with 10 μg/ml Alexa Fluor 594-conjugated wheat germ agglutinin (AF594-WGA; Invitrogen) for 10 min and washed with PBS for 10 min. AF594-WGA delineates the plasma membrane when briefly incubated with live cells (Jeng et al., 2008). The average width of the AF594-WGA fluorescence (1.5 μm in HEK293T cells) was taken as an index of the thickness of the plasma membrane.

We used two methods to quantify the ratio of plasma membrane versus cytosolic level of TRESK proteins in HEK293T cells. First, we drew four lines through the middle of the cell image and measured the pixel-by-pixel fluorescence intensities along the line. This gave us eight points of contact with the plasma membrane. We used the fluorescence intensities within 1.5 μm of the outer boundary of the cell to represent the level of TRESK proteins on the plasma membrane. The rest of the signal represented the cytoplasmic level of TRESK protein expression. Second, we manually traced the outer boundary of the fluorescent image as the perimeter of that cell. An inner curve was obtained 1.5 μm from the perimeter. The region enclosed by the two curves represented the annular membrane ROI. The region enclosed by the inner curve represented the cytoplasmic ROI. The area, total fluorescent intensity, and average intensity within the ROI were measured with the SimplePCI software (Cao et al., 2004).

Immunostaining of transfected HEK293T cells. To generate an antibody recognizing mouse TRESK channels, we inserted the peptide sequence corresponding to the 53–68 aa (SAVEGRPDPEAEENPE) of the mouse TRESK subunits into the major immune-dominant region of the hepatitis B virus core protein with a hexahistidine tag at the C terminus (Pumpens and Grens, 2001). This epitope is in the first extracellular loop of the mouse TRESK subunits. The recombinant fusion protein was expressed in *Escherichia coli* BL21(DE3)pLysS cells and the self-assembled virus-like particles was purified from the soluble fraction by the PrepEase histidine-tagged protein purification kit (Affymetrix). Adult Swiss Webster mice were immunized with 50 μg of virus-like particles every 2 weeks. Ten days after the sixth immunization, blood was collected by cardiac puncture and sera was separated from blood clot, aliquoted, and stored at −80°C. All procedures were approved by the animal studies committee at Washington University.

HEK293T cells were transfected with EGFP-tagged wild-type and/or mutant TRESK subunits and reseeded onto coverslips 1 d after transfection. At 2–3 d after transfection, cells were washed with PBS and fixed by 4% formaldehyde for 5 min followed by PBS wash. The coverslips were incubated in blocking buffer (PBS with 10% normal goat serum and 0.1% Triton X-100) for 1 h and incubated with a mouse polyclonal antibody against an extracellular domain of TRESK (1:2000) in blocking buffer at 4°C overnight. After three washes by the blocking buffer (20 min each), the coverslips were incubated with the Alexa Fluor 594-conjugated goat anti-mouse secondary antibody (1:2000; Invitrogen) in blocking buffer for 1 h and then washed again 3 times in PBS. The coverslips were mounted with Crystal Mount medium and stored at 4°C. Transfected cells were identified by EGFP fluorescence. The fluorescent images were captured and analyzed as described above.

For the surface labeling experiment, cells were washed with PBS and fixed by 4% formaldehyde at 4°C for 5 min followed by PBS wash. Triton X-100 was omitted in all solutions (Barrett et al., 2005).

Protein preparation and immunodetection. HEK293T cells were transfected with V5 epitope-tagged TRESK constructs and harvested 2 d after transfection. Cells were resuspended in Laemmli sample buffer without DTT or β-mercaptoethanol (Bio-Rad) and cell lysates were briefly sonicated 10 times. The insoluble material was removed by centrifugation at 20,000 × *g* for 10 min at 4°C. The supernatants were stored at 4°C. Proteins (10 μl of each sample) were separated on 4–20% SDS-PAGE (Bio-Rad). For determination of molecular weights, prestained molecular weight ladders (Lambda Bio) were loaded along with protein samples. Blots were transferred to PVDF membranes (Bio-Rad) for 1 h at 350 mA.

The immunodetection was performed at room temperature. The membranes were incubated in blocking buffer (Li-Cor Biosciences) for 1 h and then incubated with a rabbit polyclonal antibody against the V5 epitope (1:1000 diluted in blocking buffer; Abcam) for 1 h. After three washes by the blocking buffer (20 min each), the membranes were incubated with the IRDye 800-conjugated anti-rabbit secondary antibody (1:20,000 diluted in blocking buffer; Li-Cor Biosciences) for 1 h and

washed again 3 times in PBS. Immunoblots were scanned using the Odyssey infrared imaging system (Li-Cor Biosciences). To compare the relative amount of protein in each lane, the membranes were incubated with a mouse antibody against α-tubulin (1:500; Invitrogen) for 1 h, followed by 1 h incubation with the IRDye 700-conjugated anti-mouse secondary antibody (1:20,000 diluted in blocking buffer; Li-Cor Biosciences).

Coimmunoprecipitation. For coimmunoprecipitation (CoIP) experiments, HEK293T cells were cotransfected with HA and V5 epitope-tagged TRESK constructs. The control groups were cotransfected with HA-tagged TRESK constructs and V5-EGFP. Cells were harvested 2 d after transfection and resuspended in lysis buffer containing the following (in mM): 50 Tris-HCl pH 7.5, 150 NaCl, 2 EDTA, 2 EGTA, 1% Triton X-100, and 1% protease inhibitor mixture (Sigma). Cell lysates were briefly sonicated 10 times. The insoluble material was removed by centrifugation at 20,000 × *g* for 10 min at 4°C. The supernatants (2 ml containing 1 mg of protein) were immunoprecipitated overnight at 4°C with 50 μl of anti-V5 agarose affinity gel (Sigma). The cell lysate were removed by centrifugation at 8000 × *g* for 2 min and the agarose was washed with the lysis buffer 3 times. Immunoprecipitates were eluted with 100 μl of Laemmli sample buffer with 10 mM DTT (Bio-Rad) buffer and separated on 4–20% SDS-PAGE gels. Antibodies against V5 and HA (mouse monoclonal antibody, 1:1000; Covance) epitopes were used for immunodetection as described above.

Primary culture of neonatal mouse TG neurons and transfection. All procedures in this study were approved by the animal studies committee at Washington University. The C57BL/6 breeders were maintained on a 12 h light/dark cycle with constant temperature (23–24°C), humidity (45–50%), and food and water *ad libitum* at the animal facility of Washington University.

TG tissues were collected from postnatal day 1 mice of either sex and treated with 5 mg/ml trypsin for 15 min. Neurons were dissociated by triturating with fire-polished glass pipettes and seeded on Matrigel-coated coverslips. The MEM-based culture medium contained 5% fetal bovine serum, 25 ng/ml nerve growth factor, and 10 ng/ml glial cell line-derived neurotrophic factor and was replaced every 3 d. Neurons were transfected at 1 d *in vitro* (DIV) using Lipofectamine 2000 (Invitrogen). For electrophysiology experiments, neurons were transfected with the mtTRESK-IRES-DsRed construct or the pIRES-DsRed control plasmid. Transfected neurons were identified by the red fluorescence and recorded between 3 and 6 DIV.

For imaging analysis, neurons were transfected with EGFP-tagged TRESK constructs. Two days after transfection, neurons were incubated with AF594-WGA to delineate the plasma membrane and then fixed with 4% paraformaldehyde. Transfected neurons were identified by EGFP fluorescence. Both EGFP and AF594-WGA images were captured as described above. We manually traced the outer and inner boundaries of the AF594-WGA image of each neuron. The region enclosed by the outer and the inner curves represented total and cytoplasmic ROI, respectively. The region enclosed by the two curves represented the plasma membrane ROI. The area, total fluorescent intensity, and average intensity within the ROI were measured with the Simple PCI software.

Electrophysiology. Transfected HEK293T cells or TG neurons were identified by EGFP, DsRed, and/or mCherry fluorescence. Whole-cell patch-clamp recordings were performed at room temperature with a MultiClamp 700B amplifier (Molecular Devices). pClamp 10 (Molecular Devices) was used to acquire and analyze data. Cell capacitance and series resistance were constantly monitored throughout the recording.

Voltage-clamp experiments. The recording chamber was perfused with extracellular solution (0.5 ml/min) containing the following (in mM): 135 NaCl, 5 KCl, 2 $CaCl_2$, 1 $MgCl_2$, 5 HEPES, 10 glucose, pH 7.4 with NaOH, 310 mOsm. The pipette solution contained the following (in mM): 140 KCl, 1 EGTA, 2 $MgCl_2$, 1 ATP-Mg, 0.1 GTP-Na, 5 HEPES, 10 Tris-phosphocreatine, 10 units/ml creatine phosphokinase, pH 7.3 with KOH, 290 mOsm (Dobler et al., 2007). Recording pipettes had <3.5 MΩ resistance. Series resistance (<15 MΩ, average 8.9 ± 0.2 MΩ) was compensated by 70%. Current traces were corrected with online P/6 trace subtraction using scaled hyperpolarizing steps. Signals were filtered at 2 kHz and digitized at 10 kHz. To measure the current–voltage relationships (*I–V* curves) of K^+ channels, HEK293T cells were held at −60 mV. Command steps from −100 mV to +60 mV (10 mV increments) were applied for 500 ms and then the cell was repolarized back to −60 mV. For each cell, the peak current was normalized by the membrane capacitance (a measure of cell surface area) to reflect current density.

We also recorded whole-cell currents from small-diameter (<25 μm) TG neurons transfected with the mtTRESK-IRES-DsRed and the pIRES-DsRed control plasmids, respectively. Transfected neurons were identified by the red fluorescence and recorded between 3 and 6 DIV. The extracellular solution contained 1 μM tetrodotoxin (TTX) to inhibit TTX-sensitive Na^+ currents (Bautista et al., 2008; Tulleuda et al., 2011). Neurons were held at −60 mV and depolarized to −25 mV for 300 ms and then the potential was ramped to −135 mV at 0.2 mV/ms every 2 s (Dobler et al., 2007; Tulleuda et al., 2011). We measured the outward currents at the end of the −25 mV depolarizing step. This minimized the transient voltage-gated K^+ currents (Dobler et al., 2007). The fast TTX-resistant Na^+ currents were also completely inactivated at the end of 300 ms depolarization (data not shown). Depolarization to −25 mV only evokes very small high-voltage-activated Ca^{2+} currents, which are inactivated at the end of 300 ms depolarization (Tao et al., 2012). At −60 mV holding potential, the majority of T-type Ca^{2+} channels are inactivated (Perez-Reyes, 2003) and therefore do not contribute to the currents evoked by −25 mV depolarization. To dissect currents through TRESK channels, we bath applied 30 μM lamotrigine (Sigma) while evoking whole-cell currents using this pulse protocol (Kang et al., 2008; Tulleuda et al., 2011). Current traces were not leak subtracted in this set of experiments.

Current-clamp experiments. Neuronal excitability was studied in small-diameter TG neurons transfected with the mtTRESK-IRES-DsRed construct or the pIRES-DsRed control plasmid. The recording chamber was perfused with Tyrode's solution (0.5 ml/min) containing the following (in mM): 130 NaCl, 2 KCl, 2 $CaCl_2$, 2 $MgCl_2$, 25 HEPES, 30 glucose, pH 7.3 with NaOH, 310 mOsm. The pipette solution contained the following (in mM): 130 K-gluconate, 7 KCl, 2 NaCl, 1 MgCl2, 0.4 EGTA, 4 ATP-Mg, 0.3 GTP-Na, 10 HEPES, 10 Tris-phosphocreatine, 20 units/ml creatine phosphokinase, pH 7.3 with KOH, 290 mOsm. Recording pipettes had < 4.5 MΩ resistance. Series resistance (<20 MΩ) was not compensated. Signals were filtered at 10 kHz and digitized at 50 kHz. After establishing whole-cell access, membrane capacitance was determined with amplifier circuitry. The amplifier was then switched to current-clamp mode to measure resting membrane potential (V_{rest}). The R_{in} was calculated by measuring the change of membrane potential in response to a 20 pA hyperpolarizing or 25 pA depolarizing current injection from V_{rest}. Neurons were excluded from analysis if the V_{rest} was higher than −40 mV or R_{in} was smaller than 200 MΩ.

To test neuronal excitability, neurons were held at V_{rest} and injected with 1 s depolarizing currents in 25 pA incremental steps until at least 1 action potential (AP) was elicited. The rheobase was defined as the minimum amount of current to elicit at least 1 AP. The first AP elicited using this paradigm was used to measure AP threshold (the membrane potential at which dV/dt exceeds 10 V/s), amplitude, and half-width. The amplitude of afterhyperpolarization (AHP) was measured from the single AP elicited by injecting a 1 ms depolarizing current in 200 pA incremental steps from the V_{rest}. Data were analyzed with Clampfit (Molecular Devices) and Origin (OriginLab) software.

At the end of each electrophysiological recording, neurons were incubated with FITC-conjugated isolectin B4 (IB4; 3 μg/ml) for 10 min. The FITC fluorescence on soma membrane was detected after 10 min perfusion to wash off unbound IB4. The recording pipette remained attached to the neurons during IB4 staining and washing. The V_{rest}, R_{in}, capacitance, series resistance, and leak currents were not significantly altered after IB4 staining. None of the neurons was destroyed and/or detached from the coverslip/pipette after electrophysiological recording and/or after IB4 staining.

Statistical analysis. All data are reported as mean ± SEM. The normality of each dataset was assessed by χ^2 test. Statistical significance was assessed by a two-tailed *t* test, one-way ANOVA with *post hoc* Bonferroni test, one-way repeated-measures (RM) ANOVA with *post hoc* Dunnett

test, or two-way RM ANOVA with *post hoc* Bonferroni test where appropriate. $p < 0.05$ was considered significant.

Results

Dominant-negative effect of the KCNK18 frameshift mutation on whole-cell TRESK current

We introduced the *KCNK18* frameshift mutation into the corresponding region of the mouse TRESK cDNA and investigated whether the mutation has a similar effect on human and mouse TRESK channels. The mutation results in the premature truncation in the second transmembrane domain of both mouse and human TRESK proteins (Fig. 1*A*). First, we recorded whole-cell K^+ currents through wild-type and mutant TRESK channels in HEK293T cells. Untransfected cells exhibited very small background leak current density (35 ± 2 pA/pF at +60 mV; Fig. 1*B–D*). Cells expressing wild-type TRESK channels showed large outwardly rectifying whole-cell K^+ currents, with 457 ± 25 pA/pF current density at +60 mV (Fig. 1*B–D*). The *I–V* curve was typical of background K^+ channels (Fig. 1*C*) (Sano et al., 2003; Kang et al., 2004; Lafrenière et al., 2010). In contrast, cells expressing mutant TRESK channels only exhibited very small outward K^+ currents (53 ± 3 pA/pF at +60 mV), similar to that of the untransfected cells (Fig. 1*B–D*).

Next, we investigated whether the mutant mouse TRESK subunits exert a dominant-negative effect on whole-cell TRESK currents. Varying the amount of plasmid DNA for transfection did not significantly affect the size of wild-type TRESK current density (Fig. 1*F*,*G*, WT-4 μg vs WT-2 μg groups; $p = 0.7$, one-way ANOVA with *post hoc* Bonferroni test). When we cotransfected HEK293T cells with plasmids encoding wild-type and mutant TRESK subunits at 1:1 molar ratio, we observed a 70% reduction of the whole-cell TRESK current density, from 466 ± 23 pA/pF at +60 mV to 125 ± 6 pA/pF (Fig. 1*F*,*G*, WT-4 μg and WT-2 μg/MT-2 μg groups, respectively; $p < 0.001$), indicating that the truncated TRESK subunits cause a reduction of the wild-type TRESK channel activity. Transfection of wild-type and mutant TRESK DNA at 1:5 molar ratio did not further decrease the TRESK current (Fig. 1*G*, WT-2 μg/MT-2 μg group vs WT-0.7 μg/MT-3.5 μg group; $p = 0.4$). We conclude that the frameshift mutation has a similar dominant-negative effect on whole-cell currents through human and mouse TRESK channels (Lafrenière et al., 2010).

Wild-type and mutant TRESK subunits interact with each other in HEK293T cells

Like other K_{2P} channels, the TRESK protein is thought to form homodimers to conduct K^+ currents (Lesage et al., 1996; Honoré, 2007; Enyedi and Czirják, 2010; Brohawn et al., 2012; Enyedi et al., 2012; Miller and Long, 2012; Plant, 2012). The truncated TRESK subunits may exert the dominant-negative effect through coassembling with the wild-type subunits. To test this possibility, we tagged wild-type and mutant TRESK proteins with EGFP or mCherry at the N terminus and expressed the fusion proteins in HEK293T cells. We recorded currents through untagged and EGFP-tagged wild-type TRESK channels in parallel experiments (Fig. 2*A*, inset, untagged WT and EGFP-WT, respectively). The two *I–V* curves almost overlapped with each other, indicating that the EGFP tag does not affect the expression and/or other properties of the wild-type TRESK channels. The difference between the current densities of untagged wild-type TRESK in Figure 1 and EGFP-WT in Figure 2 are likely due to the fact that the data were collected by different experimenters with different batches of HEK293T cells and transfection reagents. Similar to the untagged mutant TRESK subunits, EGFP-MT subunits were also nonfunctional and exhibited a dominant-negative effect on whole-cell TRESK currents (Fig. 2*A*,*B*). Likewise, mCherry-WT and mCherry-MT TRESK subunits showed similar properties to those of their untagged counterparts (data not shown). In another control experiment, we expressed mCherry-WT and mCherry-MT TRESK subunits in HEK293T cells, respectively. Two days after transfection, we fixed cells and stained the nucleus with fluorescent dye DAPI. We found no overlap between the DAPI and mCherry signals, indicating that the overexpressed exogenous TRESK subunits were not misrouted to the nucleus (data not shown).

We went on to investigate whether the wild-type and mutant TRESK subunits colocalize with each other in HEK293T cells. For each transfected cell, we randomly chose 30 pixels (0.10 μm^2 per pixel) and measured the EGFP and mCherry fluorescence intensities in each pixel. We found a strong positive correlation between the EGFP and mCherry fluorescence intensities in cells coexpressing EGFP-WT and mCherry-WT and cells coexpressing EGFP-MT and mCherry-MT subunits (Fig. 2*D*,*E*,*G*). Similarly, there was a strong positive correlation between the EGFP-WT and mCherry-MT fluorescence intensities (Fig. 2*D*,*F*). As a control experiment, we coexpressed EGFP-WT TRESK with mCherry-tagged 5-HT 1F receptor (mCherry-1F), a G-protein-coupled seven-transmembrane protein. We found no correlation between the EGFP and mCherry fluorescence intensities (Fig. 2*D*,*H*). These data indicate that wild-type and mutant TRESK subunits colocalize with each other in HEK293T cells, suggesting that they may coassemble and form nonfunctional channels.

To further test this hypothesis, we tagged wild-type and mutant TRESK proteins with V5 epitope at the N terminus and expressed the fusion proteins in HEK293T cells because EGFP may self-associate to form dimers. The protein lysates were prepared and analyzed by immunoblot using a V5 antibody (Fig. 3*A*). Not taking into account the glycosylation, the predicted relative molecular weight (M_r) for V5-WT and V5-MT proteins were 44 and 22 kDa, respectively. No signal was detected from untransfected cells. We found that proteins from cells expressing V5-WT subunits exhibited a major band with M_r around 90 kDa and a very faint band around 45 kDa, corresponding to the predicted size of the wild-type TRESK dimer and monomer, respectively (Egenberger et al., 2010). This suggests that the majority of wild-type TRESK subunits remain self-assembled as dimers under our experimental conditions, as in the case of TWIK-1, another K_{2P} channel (Lesage et al., 1996). Likewise, lysates from cells expressing V5-MT subunits displayed a major band around 45 kDa and a fainter band around 25 kDa, corresponding to the predicted size of mutant TRESK dimer and monomer. Interestingly, in addition to the 90 and 45 kDa bands, we also observed a band with M_r around 63 kDa in proteins from cells coexpressing V5-WT and V5-MT TRESK subunits. This corresponds to the predicted size of the WT-MT heterodimer. Our results provide additional support to the idea that truncated TRESK subunits may exert the dominant-negative effect through coassembling with the wild-type subunits.

We also conducted CoIP experiments to confirm the interaction between TRESK subunits in HEK293T cells. To this end, we generated constructs that encode wild-type and mutant TRESK proteins with the HA epitope at the N terminus. First, we coexpressed HA-WT and V5-WT TRESK subunits in HEK293T cells. The V5 antibody pulled down a protein complex containing both V5-WT and HA-WT TRESK (Fig. 3*B*), indicating that wild-type

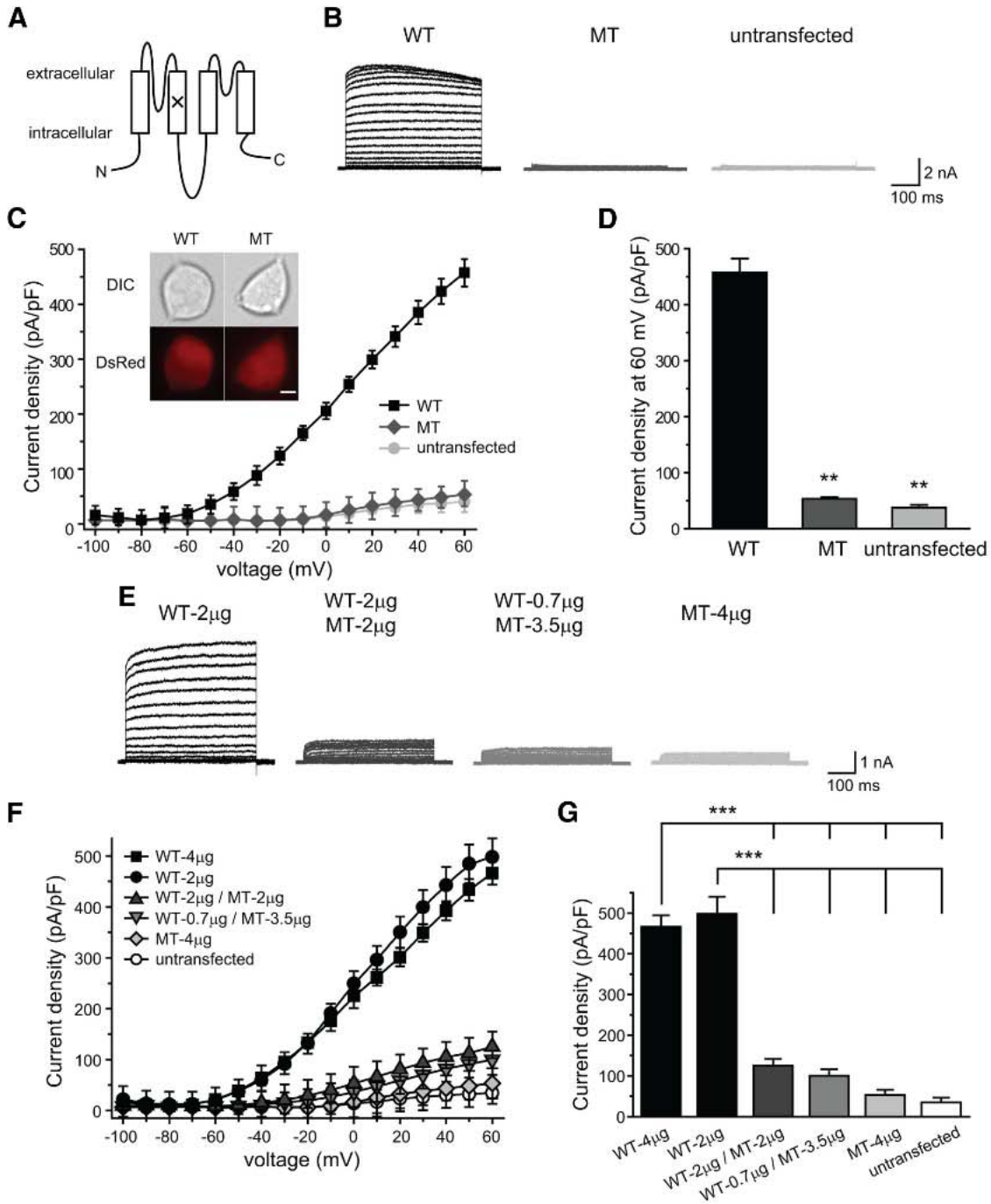

Figure 1. Dominant-negative effect of the frameshift mutation on whole-cell TRESK current in HEK293T cells. A, Topology of the mouse TRESK subunit. The location of the frameshift mutation is labeled by the "×" symbol. B, Representative current records from untransfected HEK293T cells and cells expressing wild-type (WT) or mutant (MT) TRESK channels. Cells were transfected with wtTRESK-IRES-DsRed or mtTRESK-IRES-DsRed constructs. Transfected cells were held at −60 mV and subjected to 500 ms voltage steps from −100 mV to +60 mV (10 mV increments, every 10 s) and then repolarized back to −60 mV. C, I/V curves of peak TRESK current densities in untransfected HEK293T cells and cells expressing WT or MT TRESK channels, respectively (the same recording protocols as in B, n = 10, 14, 10 cells in each group, respectively). Inset: Representative images of transfected HEK293T cells. Cells were transfected with wtTRESK-IRES-DsRed or mtTRESK-IRES-DsRed constructs and expressed DsRed protein along with WT and MT TRESK subunits, respectively. Top and bottom, DIC and DsRed fluorescent images, respectively. Scale bar, 5 μm. D, TRESK current densities at +60 mV (the same cells as in C; $^{**}p < 0.01$, one-way ANOVA with post hoc Bonferroni test vs the WT group; no statistical significance between the MT and untransfected groups). E, Representative current records from HEK293T cells expressing WT TRESK alone, MT TRESK alone, or coexpressing WT and MT TRESK subunits (the same recording protocols as in B). The amount of plasmid DNA used in each transfection is indicated. F, I/V curves of peak TRESK current densities in untransfected HEK293T cells and cells transfected with various amounts of plasmids encoding WT and MT TRESK subunits, respectively (the same recording protocols as in B, n = 10 cells in each group). G, TRESK current densities at +60 mV (the same cells as in F; $^{***}p < 0.001$ vs the WT-4 μg and the WT-2 μg groups, respectively; no statistical significance between other groups; one-way ANOVA with post hoc Bonferroni test).

TRESK subunits interact with each other in HEK293T cells. In control cells coexpressing HA-WT TRESK and V5-EGFP proteins, the V5 antibody only pulled down V5-EGFP, but not HA-WT TRESK (Fig. 3*B*). Similarly, V5-MT TRESK, but not V5-EGFP, pulled down HA-MT TRESK subunits (Fig. 3*D*), indicating that mutant TRESK subunits interact with each other in HEK293T cells. Next, we investigated whether wild-type TRESK interacts with the mutant subunits by coexpressing HA-MT and

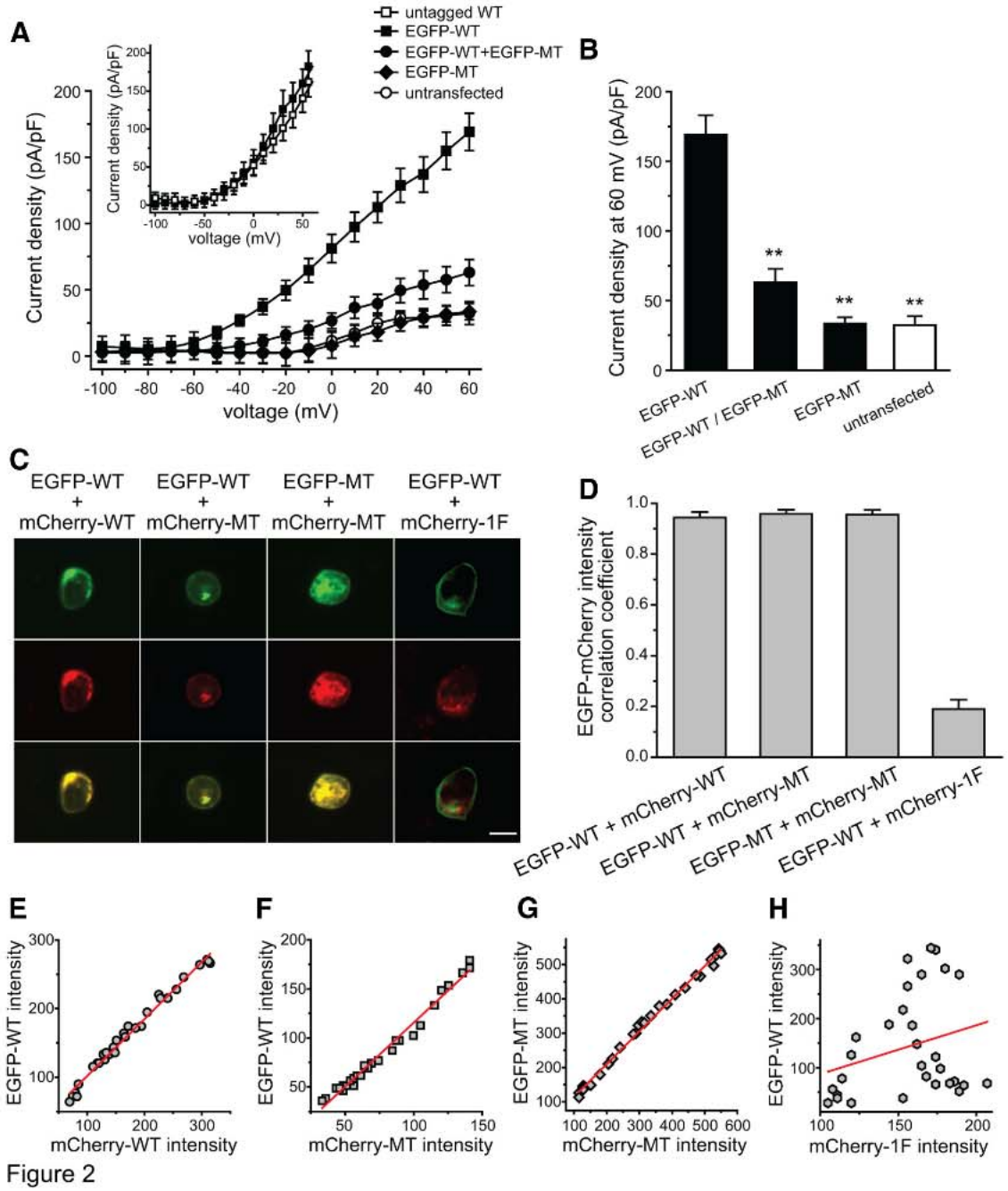

Figure 2

Figure 2. Colocalization of WT and MT TRESK subunits in HEK293T cells. A, I–V curves of peak TRESK current densities in untransfected HEK293T cells, cells expressing EGFP-WT subunits, EGFP-MT subunits, and cells coexpressing EGFP-WT and EGFP-MT TRESK subunits, respectively (the same recording protocols as in Fig. 1*A*, $n = 10–15$ cells in each group). The inset shows the I–V curves of TRESK current densities in HEK293T cells expressing untagged WT and EGFP-WT TRESK subunits in parallel experiments ($n = 4$ cells in each group), respectively. B, TRESK current densities at +60 mV (the same cells as in A; $^{**}p < 0.01$ vs the EGFP-WT group, no statistical significance between other groups; one-way ANOVA with post hoc Bonferroni test). C, Representative images of HEK293T cells coexpressing EGFP- or mCherry-tagged TRESK subunits as indicated above each column. The first column on the right contains images of a cell coexpressing EGFP-WT TRESK and mCherry-tagged 5-HT 1F receptor (mCherry-1F). Two micrograms of each plasmid was used in each transfection. Top and middle, EGFP- and mCherry-tagged protein images, respectively. Bottom, Merged images. Scale bar, 10 μm. D, Mean correlation coefficient (r) of EGFP versus mCherry fluorescence intensities in cells coexpressing EGFP- and mCherry-tagged TRESK subunits. For each cell, the value of r was calculated from pixel-by-pixel comparison of EGFP and mCherry fluorescence intensities in 30 randomly chosen pixels. The p-value was determined by the value of r and the degrees of freedom ($df = 28$). All cells in the EGFP-WT + mCherry-1F group ($n = 20$) have $p > 0.05$, indicating a lack of correlation between EGFP-WT TRESK and mCherry-1F proteins. All cells in the other three groups ($n = 20$ in each group) have $p < 0.001$, indicating a strong colocalization between WT and MT TRESK subunits in HEK293T cells. E–G, Scatterplots of EGFP versus mCherry fluorescent intensities (in arbitrary units) in 30 randomly selected pixels from three representative cells coexpressing EGFP- and mCherry-tagged TRESK subunits. Each pixel corresponds to 0.10 μm^2 area. The regression lines represent the correlation between the EGFP and mCherry intensities. H, Scatterplot of EGFP versus mCherry fluorescent intensities (in arbitrary units) in 30 randomly selected pixels from a representative cell coexpressing EGFP-WT TRESK and mCherry-1F proteins.

V5-WT TRESK subunits in HEK293T cells. Indeed, the V5 antibody pulled down a protein complex containing both V5-WT and HA-MT TRESK (Fig. 3*C*). On the contrary, the V5 antibody failed to CoIP mutant TRESK in control cells coexpressing HA-MT TRESK and V5-EGFP proteins (Fig. 3*C*). These CoIP results provided direct evidence that wild-type and mutant TRESK subunits interact with each other in HEK293T cells. The TRESK signals in Figure 3*B–D* corresponded to the monomeric

form of wild-type and mutant subunits, respectively. This was likely due to the fact that the samples were diluted in buffer containing the reducing agent DTT. Further experiments are needed to determine whether TRESK subunits form dimers via disulfate bridges, similar to the TWIK-1 K_{2P} channel (Lesage et al., 1996).

Mutant TRESK subunits reduce the plasma membrane trafficking of wild-type TRESK subunits in HEK293T cells

To investigate whether the frameshift mutation alters the expression level and/or the subcellular localization of TRESK subunits, we compared the expression level of wild-type and truncated TRESK subunits. To mimic the expression of TRESK from two alleles in human cells, we transfected HEK293T cells with EGFP- and mCherry-tagged TRESK constructs at a 1:1 ratio. To our surprise, the level of total EGFP-MT TRESK fluorescence intensity was 1.7-fold higher than that of EGFP-WT TRESK (Fig. 4*A*,*B*, EGFP-WT+mCherry-WT group vs EGFP-MT+mCherry-MT group; $p < 0.001$, one-way ANOVA with *post hoc* Bonferroni test). Interestingly, coexpression of wild-type TRESK subunits reduced the total fluorescence intensity of EGFP-MT subunits to a level comparable to that of EGFP-WT subunits (Fig. 4*B*, EGFP-MT+mCherry-WT group vs EGFP-WT+mCherry-WT group; $p = 1.0$). Conversely, coexpression of mutant TRESK did not affect the level of total EGFP-WT TRESK fluorescence intensity in HEK293T cells (Fig. 4*B*, EGFP-WT+mCherry-MT group vs EGFP-WT+mCherry-WT group; $p = 0.34$). The altered expression level of mutant TRESK subunits likely results from the mutation *per se* rather than from the N-terminal EGFP tag because we also quantified the expression level of mCherry-WT and mCherry-MT TRESK subunits and obtained similar results (data not shown, but see Fig. 4*A* for representative images).

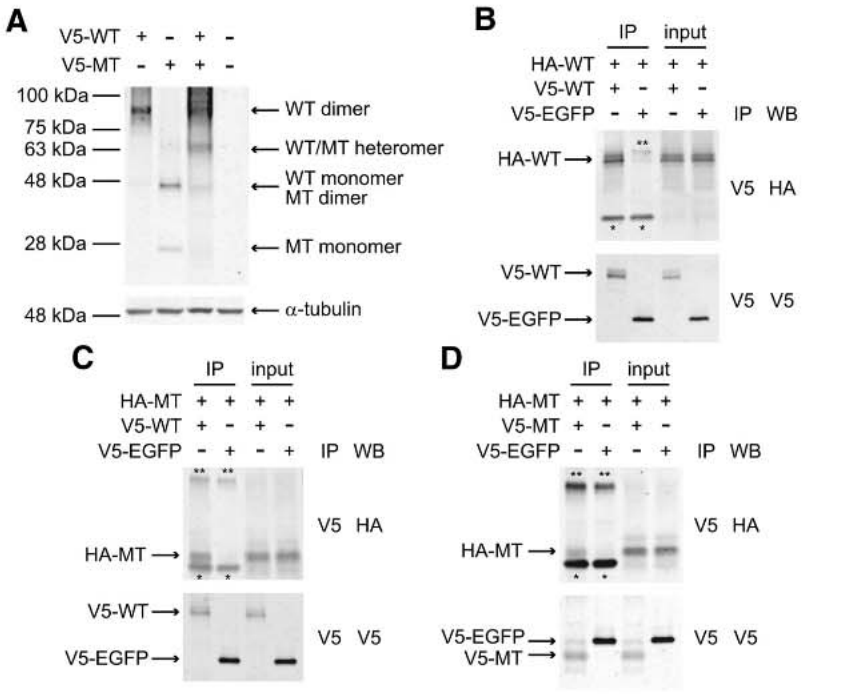

Figure 3. Wild-type and mutant TRESK subunits interact with each other in HEK293T cells. *A*, Characterization of V5-tagged WT and MT TRESK subunits in HEK293T cells by Western immunoblotting (WB). The plasmids used in each transfection are indicated above each lane. Lysate from untransfected cells is included as a control (right). V5-WT and V5-MT TRESK subunits were detected by an antibody against V5-tag. Left, M| markers. Bottom, Signal of α-tubulin on a replica membrane to indicate the relative amount of protein in each sample. The experiment was repeated multiple times. *B–D*, CoIP of V5- and HA-tagged TRESK subunits in HEK293T cells. The plasmids used in each transfection are indicated above each lane. Top, Western blot of anti-V5 immunoprecipitates (IP) and the corresponding cell lysates (input) probed with the anti-HA antibody. Bottom, Replica plots probed with the anti-V5 antibody showing the amount of V5-tagged TRESK and V5-EGFP proteins. Signals of V5- and HA-tagged TRESK subunits and IgG heavy (**) and light chains (*) are indicated.

Does the frameshift mutation affect the trafficking of wild-type and/or mutant TRESK subunits to the plasma membrane? Here we used two methods to quantify the ratio of plasma membrane versus cytosolic level of TRESK proteins in HEK293T cells (for further details, see Fig. 4 legend and Materials and Methods). First, we drew four lines through the middle of the cell image and measured the EGFP fluorescence intensities along the lines (Fig. 4*A*). We found that the plasma membrane versus cytosol ratio of EGFP-MT TRESK subunits was only 43 ± 2% of the EGFP-WT subunits, indicating that the plasma membrane insertion of the truncated TRESK subunits was significantly reduced (Fig. 4*A*,*C*, EGFP-WT+mCherry-WT group vs EGFP-MT+mCherry-MT group; $p < 0.001$, one-way ANOVA with *post hoc* Bonferroni test). Interestingly, when coexpressed in HEK293T cells, both wild-type and mutant TRESK subunits exhibited a similar reduction of the membrane versus cytosol ratio (Fig. 4*A*,*C*, EGFP-WT+mCherry-MT and EGFP-MT+mCherry-WT groups vs EGFP-WT+mCherry-WT group; $p < 0.001$). Second, we used an annular ROI to represent the plasma membrane region of a cell. In cells coexpressing EGFP-WT and mCherry-MT TRESK subunits, the plasma membrane versus cytosol ratio of EGFP-WT subunits was 0.60 ± 0.05, significantly lower than the ratio of the EGFP-WT in cells expressing wild-type TRESK alone (1.0 ± 0.1, $n = 10$ cells in each group; $p < 0.01$, *t* test). Therefore, the two methods of quantifying the efficiency of TRESK protein trafficking to the plasma membrane yielded similar results. Both are consistent with the hypothesis that, when coexpressed in HEK293T cells, mutant TRESK subunits interact with the wild-type subunits, thereby decreasing the plasma membrane trafficking of the TRESK channels.

Measuring steady-state surface expression of TRESK channels with an antibody against the extracellular domain of mouse TRESK subunits

To better investigate the effects of the *KCNK18* mutation on the surface expression of TRESK subunits, we generated a mouse polyclonal antibody against an epitope on the first extracellular loop of the mouse TRESK protein. Because this epitope is localized upstream of the frameshift mutation, we predicted that the antibody should have similar affinity to the wild-type and truncated TRESK subunits. First, we tested the specificity of the antibody by immunostaining the transfected HEK293T cells. The antibody-stained cells expressing EGFP-WT TRESK subunits. Untransfected cells and cells expressing EGFP proteins showed little staining (Fig. 5*A*). Furthermore, the TRESK-immunoreactivity (TRESK-ir) completely overlapped with the EGFP-WT TRESK fluorescence in permeabilized cells (Fig. 5*B*), indicating that the antibody specifically recognizes mouse TRESK proteins in HEK293T cells. Next, we used the antibody to detect the level of TRESK subunits on the plasma membrane. In

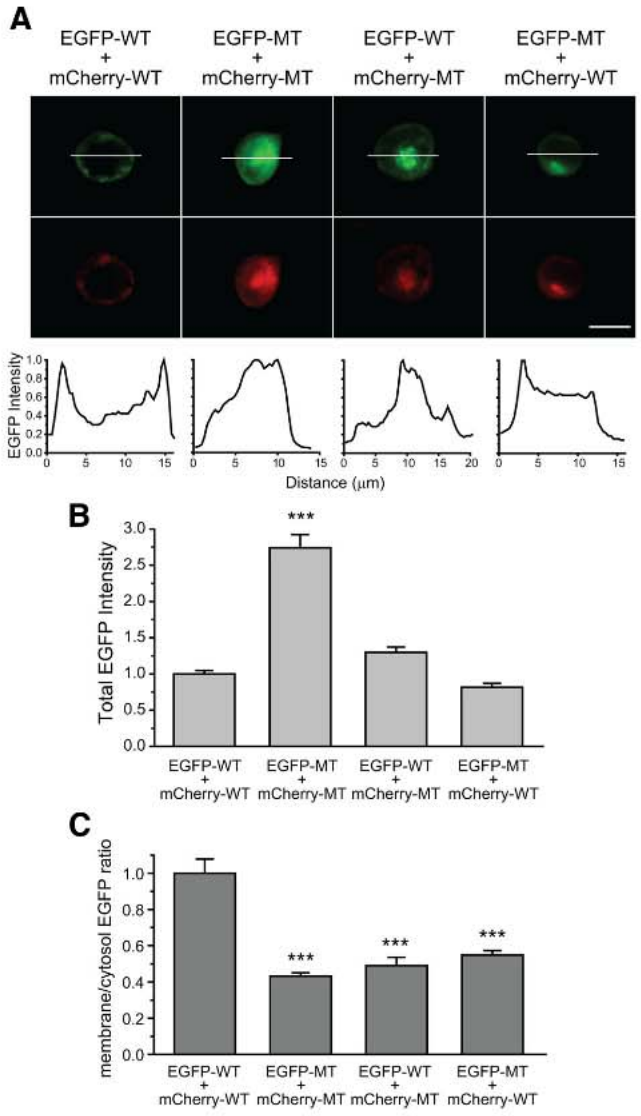

Figure 4. Total and plasma membrane levels of WT and MT TRESK subunits in HEK293T cells. A, Representative images of HEK293T cells coexpressing EGFP- and mCherry-tagged WT and MT TRESK subunits. Two micrograms of each plasmid was used in each transfection. Top and middle, EGFP- and mCherry-tagged TRESK images, respectively. Bottom, Relative EGFP fluorescence intensities along the white horizontal line through the middle of the cell. Scale bar, 10 μm. B, Total EGFP fluorescence intensity in cells expressing EGFP- and mCherry-tagged WT and MT TRESK subunits ($n = 52–60$ cells in each group; ***$p < 0.001$, one-way ANOVA with post hoc Bonferroni test vs the EGFP-WT + mCherry-WT group). C, Normalized plasma membrane versus cytosol ratio of EGFP fluorescence intensity along four lines through the middle of the cells (same cells as in B; ***$p < 0.001$, one-way ANOVA with post hoc Bonferroni test vs the EGFP-WT + mCherry-WT group). The fluorescent intensity within 1.5 μm of the outer boundary of the cell represents the level of TRESK proteins on the plasma membrane. The rest of the signal represents the cytoplasmic level of TRESK protein expression.

nonpermeabilized cells expressing EGFP-WT TRESK subunits, the EGFP signals were observed in both the plasma membrane and intracellular compartments (Fig. 5*C*, left). In contrast, TRESK-ir was restricted to the cell surface (Fig. 5*C*, middle), indicating that the antibody recognizes TRESK channels on the plasma membrane with good signal-to-noise ratio.

Cells from migraine patients with the frameshift mutation contain one wild-type and one mutant KCNK18 allele, and presumably express both wild-type and mutant TRESK subunits. To mimic this situation, we cotransfected HEK293T cells with EGFP-WT and EGFP-MT TRESK constructs at 1:1 ratio (2 μg DNA for each construct; Fig. 5*C–F*, WT+MT group). The control cells (Fig. 5*C–F*, WT group) were transfected with 4 μg of EGFP-WT constructs to mimic the expression of TRESK from two wild-type alleles in control cohorts. The value of EGFP fluorescence intensity corresponds to the expression level of total TRESK subunits in each cell. Based on the previous experiments, we predicted that cells in WT+MT group would express equal amounts of EGFP-WT and EGFP-MT TRESK subunits (Fig. 4*B*, EGFP-WT+mCherry-MT vs EGFP-MT+mCherrry-WT groups). Indeed, the relative EGFP intensity was comparable between the WT and WT+MT groups (Fig. 5*D*). Once again, we found that the EGFP level was significantly increased in cells expressing mutant TRESK alone (Fig. 5*C,D*, MT group; $p < 0.001$ compared with the WT and WT+MT groups, one-way ANOVA with *post hoc* Bonferroni test).

We went on to quantify the level of TRESK-ir on the plasma membrane. In cells expressing equal amounts of wild-type and mutant TRESK protein, the ratio of total wild-type/wild-type, mutant/mutant, and wild-type/mutant dimeric channels would be 1:1:2. Based on the data shown in Figure 4*C*, we reasoned that the efficiency of plasma membrane trafficking of both mutant/mutant homodimer and wild-type/mutant heterodimer would be ~50% of the wild-type/wild-type TRESK channels. Therefore, the ratio of wild-type/wild-type, mutant/mutant, and wild-type/mutant dimeric channels on the plasma membrane would be 2:1:2. We predicted that the level of surface TRESK-ir in the WT+MT group would be ~62.5% of that in the WT group. Indeed, our experimental data agreed very well with the predicted value. In cells coexpressing wild-type and mutant TRESK subunits, the level of surface TRESK-ir was 67 ± 6% of that in the WT group (Fig. 5*E*; $p < 0.01$, one-way ANOVA and *post hoc t* test with Bonferroni correction). After normalizing the surface TRESK-ir level with the total TRESK expression level in each cell, we found that the surface/total TRESK ratio in the WT+MT group was 69 ± 4% of the WT group (Fig. 5*F*; $p < 0.001$), again consistent with the predicted value.

The level of surface TRESK-ir was significantly higher in the MT group, likely due to the increase in total EGFP-MT protein expression (Fig. 5*E*; $p < 0.001$ compared with the WT group). Conversely, the surface/total TRESK ratio in the MT group was only 42 ± 4% of the WT group (Fig. 5*F*; $p < 0.001$ compared with the WT and WT+MT group), confirming that the plasma membrane insertion of the truncated TRESK subunits was significantly reduced.

Expression of wild-type and mutant TRESK subunits in cultured TG neurons

We compared total and plasma membrane expression of wild-type and mutant TRESK subunits in cultured TG neurons. We expressed EGFP-WT and EGFP-MT subunits in neonatal TG neurons and monitored EGFP fluorescence in the soma. Neurons in both groups exhibited diffuse EGFP fluorescence throughout the soma, both on the plasma membrane and at intracellular locations (Fig. 6*A*). In a control experiment, we expressed mCherry-WT and mCherry-MT TRESK subunits in TG neurons and stained the nucleus with DAPI. We found no overlap between the DAPI and mCherry signals, indicating that the overexpressed exogenous TRESK subunits were not misrouted to the nucleus (data not shown). Quantitative analysis showed a comparable level of somatic EGFP fluorescence intensity in TG neurons expressing EGFP-WT and EGFP-MT subunits (Fig. 6*B*). Therefore, in the presence of endogenous TRESK channels, the exogenous wild-type and truncated TRESK subunits were ex-

pressed at similar levels in TG neurons, reminiscent of what was observed in HEK293T cells (Fig. 4*B*, EGFP-WT+mCherry-WT vs EGFP-MT+mCherry-WT groups).

Next, we investigated whether the mutation affects the trafficking of TRESK subunits to the plasma membrane. We stained neurons briefly with AF594-WGA and used the WGA image as the plasma membrane ROI (Fig. 6*A*). This allowed us to measure the plasma membrane versus cytosol ratio of EGFP-tagged TRESK subunits in TG neurons. Due to the resolution limit of a light microscope, this ROI could also contain some signal from TRSK present in submembrane vesicles. We found that the ratio of EGFP-MT subunits was 67 ± 3% of the EGFP-WT subunits (Fig. 6*C*; $p < 0.01$, *t* test), indicating that the steady-state plasma membrane level of the mutant TRESK subunits was significantly reduced in TG neurons. We did not use the TRESK antibody in this set of experiments because the specificity of the antibody has not been tested against tissues from the TRESK knock-out mice and because the antibody does not discriminate the endogenous and exogenous TRESK subunits, making it impossible to calculate the surface/total expression ratio of the exogenous TRESK proteins. In a pilot experiment, we stained cultured TG neurons with the TRESK antibody and found the immunoreactivity present in the majority of TG neurons, but not non-neuronal cells (data not shown), which is consistent with previous reports (Dobler et al., 2007; Yoo et al., 2009; Lafrenière et al., 2010).

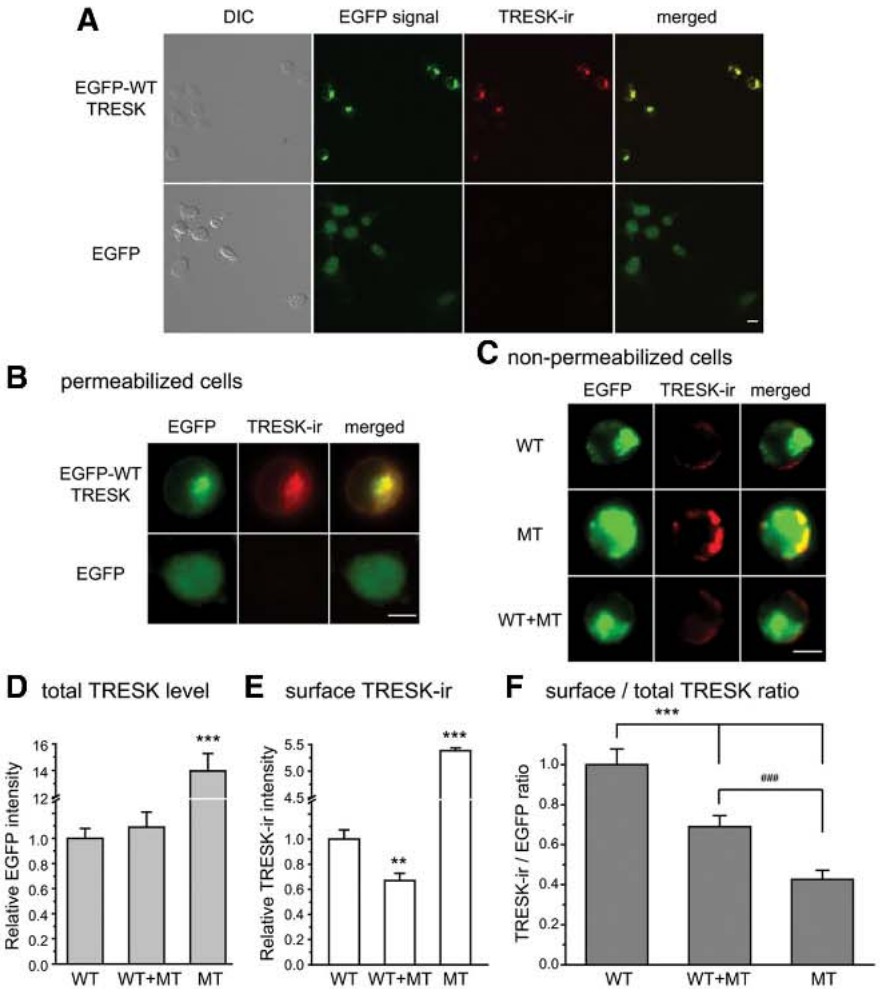

Figure 5. Coexpression of WT and MT TRESK subunits reduces the plasma membrane trafficking of TRESK channels in HEK293T cells. A,B, Representative images of HEK293T cells expressing EGFP-WT TRESK (top) and EGFP proteins (bottom), respectively. Cells were permeabilized with Triton X-100 and stained with the TRESK antibody. A, Left to right, DIC images of total cells in the field, EGFP fluorescence in transfected cells, TRESK-ir, and the merged images. B, Exemplar transfected cells at higher magnification. Scale bars: A, 10 μm; B, 5 μm. C, Representative images of HEK293T cells expressing EGFP-tagged TRESK subunits. A total of 4 μg of plasmids was used in each transfection. In WT + MT group, cells were transfected with 2 μg of EGFP-WT and 2 μg of EGFP-MT plasmids. Cells were fixed and incubated with the TRESK antibody without Triton X-100 permeabilization. Left to right, EGFP fluorescence, TRESK-ir, and the merged images. Scale bar, 5 μm. D, Total EGFP intensity in cells expressing EGFP-tagged TRESK subunits ($n = 50$ cells in each group; $^{***}p < 0.001$, one-way ANOVA with post hoc Bonferroni test vs the WT group). E, Relative surface TRESK-ir intensity in cells expressing EGFP-tagged TRESK subunits (same cells as in D; $^{**}p < 0.01$, $^{***}p < 0.001$, one-way ANOVA, post hoc t test with Bonferroni correction vs the WT group). F, Normalized surface TRESK-ir versus total EGFP intensity ratio in cells expressing EGFP-tagged TRESK subunits (same cells as in D; $^{***}p < 0.001$, one-way ANOVA with post hoc Bonferroni test vs the WT group; $^{\#\#\#}p < 0.001$, one-way ANOVA with post hoc Bonferroni test between the WT + MT and MT groups).

Mutant TRESK subunits exhibit a dominant-negative effect on endogenous TRESK currents in TG neurons

We investigated whether the truncated TRESK subunits inhibit endogenous TRESK currents in small-diameter (<25 μm) TG neurons. The majority of neurons in this TG subpopulation are primary nociceptors (Harper and Lawson, 1985a, b); a small subset of them represent the C-low threshold mechanoreceptors (Lawson et al., 1997; Seal et al., 2009). We recorded whole-cell currents from TG neurons expressing DsRed protein alone and from neurons coexpressing mutant TRESK subunits and DsRed protein (Fig. 7*A*, control and MT_TRESK groups, respectively). First, we blocked TTX-sensitive Na^+ currents with 1 μM TTX (Bautista et al., 2008; Tulleuda et al., 2011). Next, we minimized the activation of transient voltage-gated K^+, Na^+, and Ca^{2+} currents by depolarizing neurons from −60 mV holding potential to −25 mV for 300 ms and subsequently hyperpolarizing neurons to −135 mV with a slow ramp (0.2 mV/ms, Fig. 7*B*; Dobler et al., 2007; Tulleuda et al., 2011). Currents measured at the end of the depolarizing step were predominantly outward K^+ currents (Dobler et al., 2007). To further dissect currents through TRESK channels, we measured the percentage of outward currents that was sensitive to 30 μM lamotrigine blockade. Previous studies show that this dose of lamotrigine inhibits TRESK currents by ~50% (Kang et al., 2008; Tulleuda et al., 2011). The reversal potentials of lamotrigine-sensitive currents in the control and MT_TRESK groups were −88 ± 5 mV and −86 ± 2 mV, respectively. This is very close to the calculated Nernst potential for K^+ currents (−84 mV) under our recording conditions. In TG neurons expressing DsRed protein alone, 39 ± 3% of the outward currents were inhibited by lamotrigine (Fig. 7*C*), similar to what was observed in DRG neurons (Kang et al., 2008; Tulleuda et al., 2011). The fraction of lamotrigine-sensitive currents was significantly lower in TG neurons expressing mutant TRESK subunits (14 ± 2%; $p < 0.05$, *t* test, Fig. 7*C*). We conclude

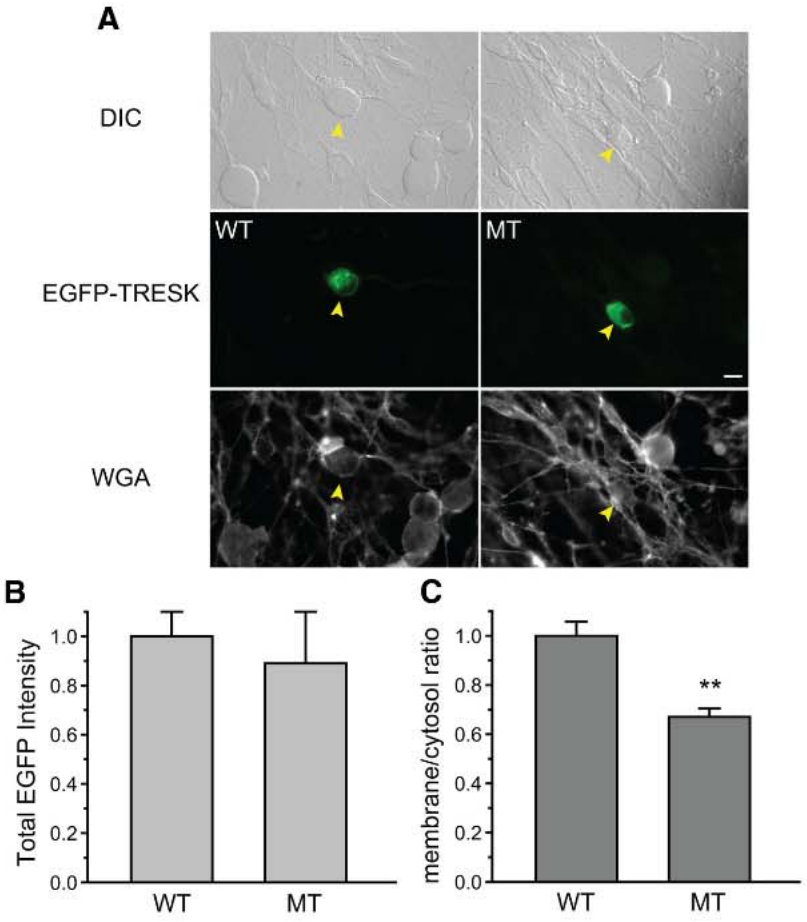

Figure 6. Total and surface expression of WT and MT TRESK subunits in TG neurons. A, Representative images of TG neurons expressing EGFP-tagged WT and MT TRESK subunits. Top, middle, and bottom, Differential interference contrast (DIC), EGFP, and AF594-WGA fluorescent images, respectively. Arrowheads indicate transfected neurons. Scale bar, 10 μm. B, Total EGFP fluorescence intensity in TG neurons expressing EGFP-tagged WT and MT TRESK subunits (n = 23 and 16 neurons, respectively). C, Normalized plasma membrane versus cytosol ratio of EGFP fluorescence intensity in TG neurons expressing EGFP-tagged WT and MT TRESK subunits (same neurons as in B). **$p < 0.01$, two-tailed t test).

that the mutant TRESK subunits exhibit a dominant-negative effect on endogenous TRESK currents in TG neurons.

Expression of mutant TRESK subunits increases R_{in} in TG neurons

Our data in TG neurons and previous studies in DRG neurons both indicate that TRESK channels contribute to the background K^+ currents in primary afferent sensory neurons (Kang and Kim, 2006; Dobler et al., 2007). We therefore investigated whether mutant TRESK subunits affect the electrophysiological properties of TG neurons. To this end, we coexpressed mutant TRESK subunits and DsRed proteins in cultured neonatal TG neurons and measured V_{rest} and R_{in} under current-clamp mode. We found that the expression of mutant TRESK subunits did not alter the V_{rest} in TG neurons (Table 1). This is consistent with a previous study showing comparable V_{rest} in DRG neurons from wild-type and TRESK G339R functional knock-out mice (Dobler et al., 2007).

Next, we injected neurons at V_{rest} with a 25 pA depolarizing current to measure R_{in}. This led to a 12 mV increase in membrane potential in control neurons, from -53.5 ± 0.3 mV to -41.5 ± 0.2 mV ($n = 25$ neurons). In TG neurons expressing mutant TRESK subunits, injection of the same depolarizing current altered the membrane potential from -52.4 ± 0.3 mV to -36.8 ± 0.4 mV, a level significantly higher than that in the control group ($n = 23$ neurons; $p < 0.05$, t test). Therefore, the R_{in} of mutant TRESK-expressing neurons was significantly higher than that of the control neurons (626 ± 13 and 479 ± 9 MΩ, respectively; $p < 0.05$, t test). We also measured R_{in} by injecting the same neurons at V_{rest} with a 20 pA hyperpolarizing current. Interestingly, the R_{in} values of control neurons and neurons expressing mutant TRESK subunits were comparable in this case (1125 ± 264 and 1244 ± 147 MΩ, respectively; $p = 0.71$, t test). This is consistent with the outward rectification of TRESK channels in physiological solutions (Fig. 1C; Enyedi and Czirják, 2010). It is likely that, under our recording conditions, there was little endogenous TRESK channel activity when membrane potential was at or below the V_{rest}. Therefore, the expression of mutant TRESK subunits does not affect the V_{rest}. However, the endogenous TRESK current is increased upon depolarization and contributes to the change of membrane potential. Here, mutant TRESK subunits exhibited a dominant-negative effect on the leak K^+ currents, caused an increase in R_{in}, and would likely affect neuronal excitability.

Expression of mutant TRESK subunits increases the excitability of TG neurons.

Upon depolarization, TG neurons expressing mutant TRESK subunits exhibit a higher R_{in} than the control neurons. This should, all else being equal, result in a lower rheobase (the current threshold to elicit AP). To determine the rheobase, we held neurons at V_{rest} and injected 1 s depolarizing currents at 25 pA incremental steps to elicit APs. To account for the heterogeneity of cultured TG neurons, we further divided the small-diameter neurons based on their ability to bind to fluorescently labeled IB4 at the end of each current-clamp recording. Previous studies have shown that the small IB4-positive and IB4-negative primary afferent neuron exhibit distinct properties in the level of neuropeptides, the termination of central projection, the encoding spike frequency, and pain modalities (Snider and McMahon, 1998; Stucky and Lewin, 1999; Choi et al., 2007; Cavanaugh et al., 2009; Scherrer et al., 2009).

Compared with neurons expressing DsRed protein (Fig. 8, control group), the mean rheobase was 50% lower in neurons expressing mutant TRESK subunits (Fig. 8, MT_TRESK group) regardless of their ability to bind to IB4 (Fig. 8*A*,*C*; $p < 0.05$, t test). In addition, a decrease of the AP voltage threshold occurred in the IB4-negative, but not IB4-positive, TG neurons expressing mutant TRESK subunits (Fig. 8*B*,*D*; $p < 0.01$, t test). Conversely, the expression of mutant TRESK subunits did not alter AP amplitude, half-width, or AHP amplitude to any significant degree (Table 1), suggesting that the endogenous TRESK currents do not play a major role in the AP repolarization process in TG neurons.

Does the expression of mutant TRESK subunits affect the spike frequency in TG neurons? First, we compared the number of APs generated by current injections from 25 to 150 pA in small

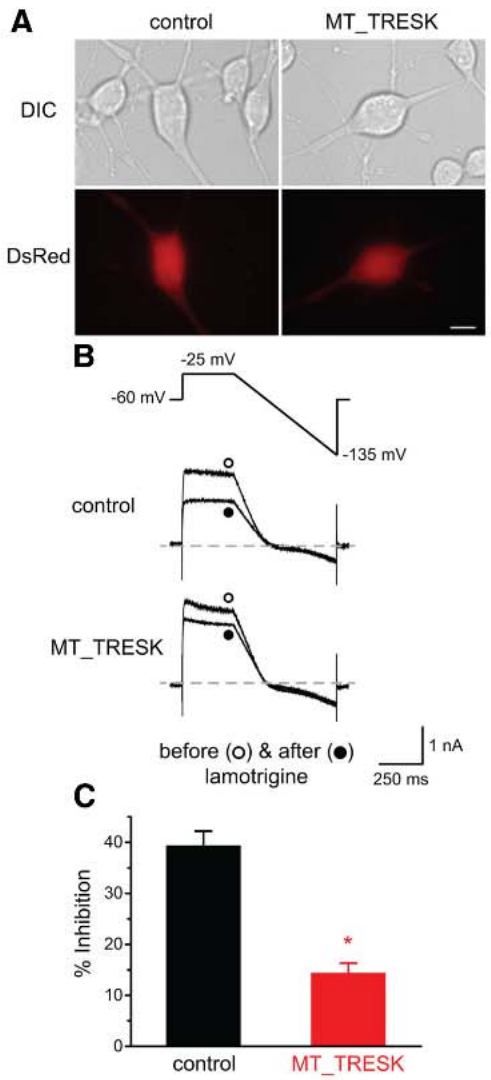

Figure 7. Decrease of lamotrigine-sensitive outward currents in TG neurons expressing MT TRESK subunits. A, Representative images of transfected TG neurons. TG neurons in the control group are transfected with the pIRES2-DsRed-Express2 plasmid and express DsRed protein alone. The MT_TRESK group contains TG neurons transfected with the mtTRESK-IRES-DsRed constructs and coexpressing DsRed protein and MT TRESK subunits. Top and bottom, DIC and DsRed fluorescent images, respectively. Scale bar, 10 μm. B, Top, Voltage protocol used to minimize transient voltage-gated K^+, Na^+ and Ca^{2+} currents. Middle and bottom, Representative current traces before and after the application of 30 μM lamotrigine. C, The percentage of outward currents (measured at the end of the depolarizing step) inhibited by lamotrigine in the control group and TG neurons expressing MT TRESK subunits (*$p < 0.05$, two-tailed t test, $n = 10$ cells in each group).

IB4-negative and IB4-positive neurons in the control group. In small IB4-negative TG neurons, the number of APs increased almost linearly in response to incremental suprathreshold current injection (Fig. 8*E*, control group; $p < 0.05$ at 125 pA and $p < 0.01$ at 150 pA, one-way RM ANOVA with *post hoc* Dunnett test vs 75 pA current injection). Conversely, 73% of the small IB4-positive neurons (8 of 11) generated a single spike in response to both threshold and suprathreshold current injections, as indicated by the flat input–output curve (Fig. 8*F*, control group; $p = 0.56$, one-way RM ANOVA). This is consistent with the results of a previous study on the difference in spike frequency between small IB4-negative and IB4-positive DRG neurons (Choi et al., 2007).

Next, we measured the spike frequency in neurons expressing mutant TRESK subunits. We found that the number of evoked APs increased significantly in response to suprathreshold current injection regardless of their ability to bind to IB4 (Fig. 8*E*,*F*, MT_TRESK groups; $p < 0.01$ at 125 pA and $p < 0.001$ at 150 pA, respectively; one-way RM ANOVA with *post hoc* Dunnett test vs 50 pA current injection in each group). Ninety percent of the IB4-positive neurons expressing mutant TRESK (9 of 10) generated multiple spikes in response to suprathreshold stimuli ($p < 0.001$, Fisher's exact test). Compared with the control neurons, the expression of mutant TRESK subunits significantly increased the number of spikes evoked by 1 s current injections in both small IB4-negative and IB4-positive neurons (Fig. 8*E*,*F*; $p < 0.05$, two-way RM ANOVA). Because there was a linear relationship between the number of APs evoked in response to current injections between 50 and 150 pA in all experimental groups, we calculated the slope of the input–output curve of each neuron. Indeed, the slope was significantly higher in neurons expressing mutant TRESK subunits relative to that of the corresponding control neurons (Fig. 8*E*,*F*, insets; $p < 0.05$, two-tailed t test). We conclude that the endogenous TRESK currents control the onset and the frequency of APs in small-diameter TG neurons and the frameshift mutation results in hyperexcitability of these neurons.

Discussion

In this study, we investigated the effects of a frameshift *KCNK18* mutation on TRESK currents and TG neuronal excitability. We introduced the mutation into the mouse TRESK subunits and found that it resulted in nonfunctional channels in HEK293T cells. Compared with cells expressing wild-type TRESK channels, coexpressing wild-type and mutant TRESK subunits at 1:1 ratio results in ~80% reduction of the current density. This is close to the predicted 75% current reduction for a dominant-negative mutation, but is more robust than the 50% reduction described previously (Lafrenière et al., 2010). The difference may reside in the different expression systems, recording protocols, and/or the species of TRESK subunits used in the two studies. We have shown here that wild-type and mutant TRESK subunits interact with each other and form dimers in HEK293T cells. Interestingly, the mutation also exhibits dominant-negative effect on the level of TRESK channels on the plasma membrane. Our results support the idea that wild-type and mutant TRESK subunits coassemble into heterodimeric channels that are nonfunctional and are also less efficient in trafficking to the plasma membrane. More experiments are needed to fully understand the physiological importance of the dominant-negative effect of mutant TRESK subunits on channel trafficking.

One important and as yet unanswered question is whether and how mutant TRESK subunits contribute to migraine pathophysiology. We reason that a good starting point is to study the function of mutant TRESK subunits in cultured TG neurons. The cell bodies of the primary afferent neurons in the trigeminal nociceptive pathway underlying migraine headache are predominantly localized in the TG. Their peripheral terminals innervate the dura and the cerebral vessels. Activation and sensitization of these neurons is a crucial step in the pathogenesis of a headache attack (Strassman et al., 1996; Bove and Moskowitz, 1997; Burstein, 2001; Harriott and Gold, 2009; Yan et al., 2011). TRESK mRNA and protein are abundantly expressed in the majority of, if not all, primary afferent neurons (Bautista et al., 2008; Yoo et al., 2009; Lafrenière et al., 2010). Previous studies show that TRESK channels contribute to background K^+ currents in DRG neurons and, in turn, regulate neuronal excitability in normal and disease states (Kang and Kim, 2006; Dobler et al., 2007; Tulleuda et al., 2011; Marsh et al., 2012; Plant, 2012). Here, we provide evidence

Table 1. Intrinsic properties of small-diameter TG neurons expressing mutant TRESK subunits

	Diameter (μm)	Capacitance (pF)	R_{in} (MΩ)	V_{rest} (mV)	Rheobase (pA)	AP threshold (mV)	AP amplitude (mV)	AP half-width (ms)	AHP amplitude (mV)	Cell number
IB4-negative neurons										
Control	20.3 ± 0.2	25.2 ± 0.7	942 ± 78	−52.9 ± 0.5	75.0 ± 3.0	−14.4 ± 0.6	112.2 ± 1.4	4.9 ± 0.2	−14.2 ± 0.5	14
Mutant	19.5 ± 0.2	22.5 ± 0.7	1123 ± 48	−52.1 ± 0.6	38.5 ± 1.8*	−23.2 ± 0.6*	107.9 ± 2.1	4.5 ± 0.3	−12.0 ± 0.4	12
IB4-positive neurons										
Control	19.9 ± 0.2	22.4 ± 1.0	1358 ± 166	−53.5 ± 0.7	77.3 ± 4.5	−17.1 ± 0.9	104.4 ± 2.4	4.6 ± 0.1	−14.9 ± 0.5	11
Mutant	18.6 ± 0.2	19.5 ± 0.7	1388 ± 94	−52.4 ± 0.6	40.0 ± 2.3*	−18.7 ± 1.2	113.3 ± 2.2	4.1 ± 0.2	−15.4 ± 0.3	10

Neurons in the control group express DsRed protein alone; the mutant group contains TG neurons coexpressing DsRed protein and MT TRESK subunits. R_{in} was calculated by measuring the change of membrane potential in response to a 20 pA hyperpolarizing current injection from V_{rest}. *$p < 0.05$ compared with the corresponding control group by two-tailed *t* test.

that mutant TRESK subunits inhibit the function of endogenous TRESK channels in TG neurons. Moreover, our results indicate that the endogenous TRESK channels are activated during subthreshold depolarization and contribute to the increase in outward conductance, which in turn counteracts the membrane depolarization. Conversely, mutant TRESK subunits inhibit endogenous TRESK currents, reduce membrane conductance (i.e., increase R_{in}), and therefore enhance the magnitude of depolarization. We have also shown that there is little endogenous TRESK channel activity when membrane potential is at or below the V_{rest}. Therefore, the V_{rest} was not altered in neurons expressing mutant TRESK subunits, which is in agreement with the results of a previous study (Dobler et al., 2007).

Conversely, other background K^+ currents may compensate for the reduction of endogenous TRESK currents in neurons expressing mutant TRESK subunits, causing an underestimation of the contribution of endogenous TRESK currents to V_{rest}. It will be interesting to determine whether acute inhibition of endogenous TRESK channels will alter V_{rest} in primary afferent neurons when TRESK-specific blockers become available in the future.

Our data predict hyperexcitability of TG neurons expressing mutant TRESK subunits. Indeed, the current threshold (rheobase) to induce AP is significantly lower in these neurons relative to the control group. Moreover, the spike frequency in response to suprathreshold stimuli was significantly increased in neurons expressing mutant TRESK subunits. This is consistent with a previous study suggesting that decrease of TRESK currents contribute to the hyperexcitability of DRG neurons in the setting of nerve injury (Tulleuda et al., 2011). Given that the AP amplitude, AP half-width, and AHP amplitude were not altered to any significant degree in these neurons, we conclude that the endogenous TRESK currents regulate the excitability of small-diameter TG neurons mainly during the rising phase of the AP waveform.

Our data obtained from transfected, cultured TG neurons from neonatal mice should be interpreted with caution given the limitations of the experimental system. However, our results are consistent with the results of a previous study of adult DRG neurons from the TRESK functional knock-out mice. Dobler et al. (2007) reported a reduction of background K^+ current, a decrease of rheobase, and normal V_{rest} in these neurons relative to the wild-type DRG neurons. Therefore, the frameshift *KCNK18* mutation likely would result in hyperexcitability of adult TG neurons as well. More experiments are necessary to test this hypothesis directly. It is unlikely that we overestimated the dominant-negative effect of mutant TRESK subunits due to overexpression because the amplitude of TRESK currents was similar in HEK293T cells transfected with wild-type and mutant TRESK DNA at a 1:1 and 1:5 molar ratio, respectively (Fig. 1*F*,*G*). Conversely, the AP width was reduced and the AHP amplitude was increased in the adult knock-out DRG neurons, whereas these parameters were not altered in neonatal TG neurons expressing mutant TRESK. It is possible that the reduction of TRESK current results in different compensatory changes of other K^+ channels in DRG and TG neurons. Alternatively, the AP width and the AHP amplitude changes may require a *de novo* and/or a prolonged absence of TRESK currents until adulthood.

We have shown previously that the familial hemiplegic migraine type 1 (FHM-1) mutation T666M results in hyperexcitability of small IB4-negative TG neurons through alteration of voltage-gated Ca^{2+} channel activities (Tao et al., 2012). The fact that both Ca^{2+} and K^+ channel mutations associated with migraine cause hyperexcitation of TG neurons suggests that the onset of migraine headache may result from abnormal membrane conductance changes of the primary afferent neurons in response to various migraine triggers. Expression of the mutant TRESK subunits increases the excitability of both small-diameter IB4-negative and IB4-positive TG neurons. We have shown in a previous study that, under our culture conditions, the majority of the small IB4-negative TG neurons express calcitonin gene-related peptide (CGRP), a neuropeptide that plays important role in migraine pathophysiology (Ho et al., 2010; Tao et al., 2012). A small fraction of IB4-negative neurons that do not express CGRP (9% of cultured TG neurons; Tao et al., 2012) may correspond to the C-low threshold mechanorecepetor (Lawson et al., 1997; Seal et al., 2009; Li et al., 2011). The contribution of these neurons to migraine pathophysiology is not well studied and they likely represent <10% of transfected neurons in our study. Conversely, IB4-positive TG neurons express little or very low levels of neuropeptides (Snider and McMahon, 1998; Stucky and Lewin, 1999; Tao et al., 2012), but many of them express $P2X_3$ receptors and mediate the pronociceptive effects of ATP, which is involved in migraine pathophysiology (Ruan et al., 2004; Staikopoulos et al., 2007). The dural afferent neurons contain both IB4-negative and IB4-positive populations (Huang et al., 2012), raising the possibility that mutant TRESK subunits may exert a dominant-negative effect on the endogenous TRESK currents and increase the excitability of primary afferent neurons in the migraine circuit. In addition, mutant TRESK subunits may affect the excitability of medium- and large-sized primary afferent neurons that express TRESK channels. Our results also suggest that TRESK channels may be a promising therapeutic target for migraine headache and other orofacial pain. Indeed, overexpressing TRESK subunits in cultured DRG neurons inhibits capsaicin-evoked substance P release (Zhou et al., 2012). Given that TRESK channel activity can be modulated by pH, anesthetics, and various intracellular signaling pathways, the recent molecular modeling study may help to facilitate structure-based design of TRESK channel openers and/or modulators (Enyedi and Czirják, 2010; Brohawn et al., 2012; Enyedi et al., 2012; Miller and Long, 2012; Rahm et al., 2012; Kim et al., 2013).

In addition to TG and DRG neurons, TRESK mRNA is expressed in many regions of the peripheral nervous system and the

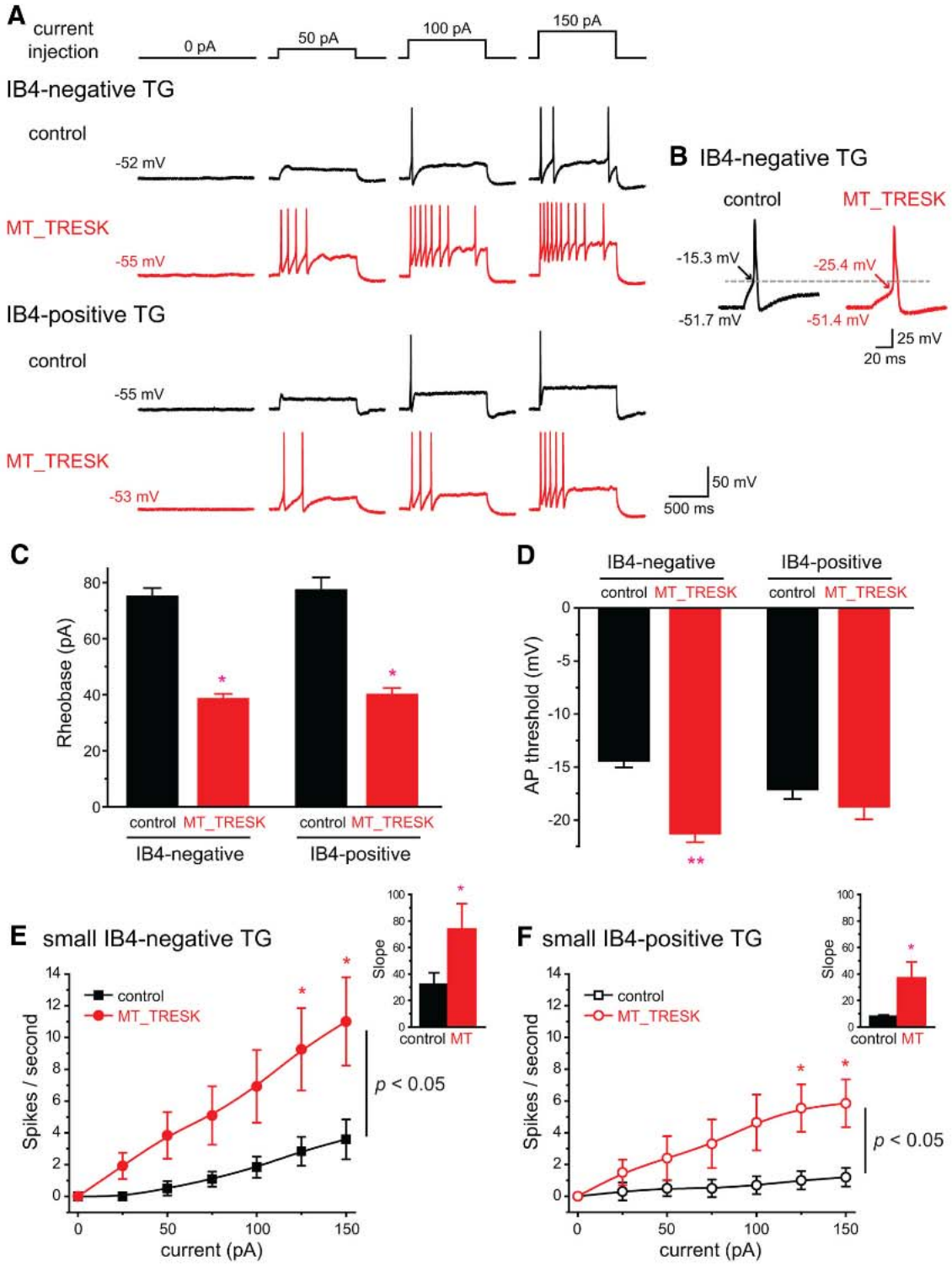

Figure 8. Neuronal excitability is increased in small TG neurons expressing mutant TRESK subunits. A, Representative traces of APs generated by incremental depolarizing current injections in transfected, small-diameter TG neurons. Neurons in the control group express DsRed protein alone. The MT_TRESK group contains TG neurons coexpressing DsRed protein and MT TRESK subunits. The values of V_{rest} are indicated for each neuron. B, Representative traces of the first AP generated by current injections at the rheobase in two transfected small IB4-negative TG neurons. Arrows indicate the AP threshold (the membrane potential at which dV/dt exceeds 10 V/s). The values of V_{rest} and the AP threshold are indicated for each neuron. C, Mean rheobase of the transfected, small-diameter TG neurons (*$p < 0.05$, two-tailed t test between the corresponding control and MT_TRESK groups, $n = 10–14$ neurons in each group). D, Mean AP threshold of transfected, small-diameter TG neurons (same cells as in C; **$p < 0.01$, two-tailed t test between the corresponding control and MT_TRESK groups). E, F, Input–output plots of the spike frequency in response to 1 s depolarizing current injections in 25 pA incremental steps in transfected, small IB4-negative (E) and IB4-positive (F) TG neurons (*$p < 0.05$ between the corresponding control and MT_TRESK groups, two-way RM ANOVA and post hoc test with Bonferroni correction; same neurons as in C). Insets: Slope of the input–output relationships between 50 pA and 150 pA current injections. *$p < 0.05$, two-tailed t test.

CNS (Sano et al., 2003; Kang et al., 2004; Dobler et al., 2007; Yoo et al., 2009). Patients carrying the frameshift mutation suffer from migraine with aura. It will be interesting to determine whether the mutation affects cortical spreading depression, the substrate of aura. Likewise, more experiments are needed to investigate whether the endogenous TRESK channels regulate the activity of cells involved in migraine pathophysiology and regulate the gain of the neuronal circuit underlying migraine.

In summary, our data show a dominant-negative effect of the frameshift *KCNK18* mutation on the whole-cell TRESK currents and the plasma membrane localization of TRESK channels. Importantly, the expression of mutant TRESK subunits in TG neurons resulted in a decrease of the endogenous TRESK current, an increase in R_{in}, and, consequently, an increase in neuronal excitability. Our results suggest a possible scenario through which the TRESK mutation increases the excitability of the trigeminal nociceptive pathway, which ultimately leads to a higher susceptibility of migraine headache.

References

Andres-Enguix I, Shang L, Stansfeld PJ, Morahan JM, Sansom MS, Lafrenière RG, Roy B, Griffiths LR, Rouleau GA, Ebers GC, Cader ZM, Tucker SJ (2012) Functional analysis of missense variants in the TRESK (KCNK18) K channel. Sci Rep 2:237. CrossRef Medline

Barrett CF, Cao YQ, Tsien RW (2005) Gating deficiency in a familial hemiplegic migraine type 1 mutant P/Q-type calcium channel. J Biol Chem 280:24064–24071. CrossRef Medline

Bautista DM, Sigal YM, Milstein AD, Garrison JL, Zorn JA, Tsuruda PR, Nicoll RA, Julius D (2008) Pungent agents from Szechuan peppers excite sensory neurons by inhibiting two-pore potassium channels. Nat Neurosci 11:772–779. CrossRef Medline

Bove GM, Moskowitz MA (1997) Primary afferent neurons innervating guinea pig dura. J Neurophysiol 77:299–308. Medline

Brohawn SG, del Mármol J, MacKinnon R (2012) Crystal structure of the human K2P TRAAK, a lipid- and mechano-sensitive K^+ ion channel. Science 335:436–441. CrossRef Medline

Burstein R (2001) Deconstructing migraine headache into peripheral and central sensitization. Pain 89:107–110. CrossRef Medline

Cao YQ, Piedras-Rentería ES, Smith GB, Chen G, Harata NC, Tsien RW (2004) Presynaptic Ca^{2+} channels compete for channel type-preferring slots in altered neurotransmission arising from Ca^{2+} channelopathy. Neuron 43:387–400. CrossRef Medline

Cavanaugh DJ, Lee H, Lo L, Shields SD, Zylka MJ, Basbaum AI, Anderson DJ (2009) Distinct subsets of unmyelinated primary sensory fibers mediate behavioral responses to noxious thermal and mechanical stimuli. Proc Natl Acad Sci U S A 106:9075–9080. CrossRef Medline

Choi JS, Dib-Hajj SD, Waxman SG (2007) Differential slow inactivation and use-dependent inhibition of Nav1.8 channels contribute to distinct firing properties in $IB4^+$ and IB4 DRG neurons. J Neurophysiol 97:1258–1265. CrossRef Medline

De Fusco M, Marconi R, Silvestri L, Atorino L, Rampoldi L, Morgante L, Ballabio A, Aridon P, Casari G (2003) Haploinsufficiency of ATP1A2 encoding the Na^+/K^+ pump alpha2 subunit associated with familial hemiplegic migraine type 2. Nat Genet 33:192–196. CrossRef Medline

Dichgans M, Freilinger T, Eckstein G, Babini E, Lorenz-Depiereux B, Biskup S, Ferrari MD, Herzog J, van den Maagdenberg AM, Pusch M, Strom TM (2005) Mutation in the neuronal voltage-gated sodium channel SCN1A in familial hemiplegic migraine. Lancet 366:371–377. CrossRef Medline

Dobler T, Springauf A, Tovornik S, Weber M, Schmitt A, Sedlmeier R, Wischmeyer E, Döring F (2007) TRESK two-pore-domain K^+ channels constitute a significant component of background potassium currents in murine dorsal root ganglion neurones. J Physiol 585:867–879. CrossRef Medline

Egenberger B, Polleichtner G, Wischmeyer E, Döring F (2010) N-linked glycosylation determines cell surface expression of two-pore-domain K^+ channel TRESK. Biochem Biophys Res Commun 391:1262–1267. CrossRef Medline

Enyedi P, Czirják G (2010) Molecular background of leak K^+ currents: two-pore domain potassium channels. Physiol Rev 90:559–605. CrossRef Medline

Enyedi P, Braun G, Czirják G (2012) TRESK: the lone ranger of two-pore domain potassium channels. Mol Cell Endocrinol 353:75–81. CrossRef Medline

Harper AA, Lawson SN (1985a) Electrical properties of rat dorsal root ganglion neurones with different peripheral nerve conduction velocities. J Physiol 359:47–63. Medline

Harper AA, Lawson SN (1985b) Conduction velocity is related to morphological cell type in rat dorsal root ganglion neurones. J Physiol 359:31–46. Medline

Harriott AM, Gold MS (2009) Electrophysiological properties of dural afferents in the absence and presence of inflammatory mediators. J Neurophysiol 101:3126–3134. CrossRef Medline

Ho TW, Edvinsson L, Goadsby PJ (2010) CGRP and its receptors provide new insights into migraine pathophysiology. Nat Rev Neurol 6:573–582. CrossRef Medline

Honoré E (2007) The neuronal background K2P channels: focus on TREK1. Nat Rev Neurosci 8:251–261. CrossRef Medline

Huang D, Li S, Dhaka A, Story GM, Cao YQ (2012) Expression of the transient receptor potential channels TRPV1, TRPA1 and TRPM8 in mouse trigeminal primary afferent neurons innervating the dura. Mol Pain 8:66. CrossRef Medline

Jeng CJ, Sun MC, Chen YW, Tang CY (2008) Dominant-negative effects of episodic ataxia type 2 mutations involve disruption of membrane trafficking of human P/Q-type Ca^{2+} channels. J Cell Physiol 214:422–433. CrossRef Medline

Kang D, Kim D (2006) TREK-2 (K2P10.1) and TRESK (K2P18.1) are major background K^+ channels in dorsal root ganglion neurons. Am J Physiol Cell Physiol 291:C138–146. CrossRef Medline

Kang D, Mariash E, Kim D (2004) Functional expression of TRESK-2, a new member of the tandem-pore K^+ channel family. J Biol Chem 279:28063–28070. CrossRef Medline

Kang D, Kim GT, Kim EJ, La JH, Lee JS, Lee ES, Park JY, Hong SG, Han J (2008) Lamotrigine inhibits TRESK regulated by G-protein coupled receptor agonists. Biochem Biophys Res Commun 367:609–615. CrossRef Medline

Kim S, Lee Y, Tak HM, Park HJ, Sohn YS, Hwang S, Han J, Kang D, Lee KW (2013) Identification of blocker binding site in mouse TRESK by molecular modeling and mutational studies. Biochim Biophys Acta 1828:1131–1142. CrossRef Medline

Lafrenière RG, Rouleau GA (2011) Migraine: Role of the TRESK two-pore potassium channel. Int J Biochem Cell Biol 43:1533–1536. CrossRef Medline

Lafrenière RG, Rouleau GA (2012) Identification of novel genes involved in migraine. Headache 52:107–110. CrossRef Medline

Lafrenière RG, Cader MZ, Poulin JF, Andres-Enguix I, Simoneau M, Gupta N, Boisvert K, Lafrenière F, McLaughlan S, Dubé MP, Marcinkiewicz MM, Ramagopalan S, Ansorge O, Brais B, Sequeiros J, Pereira-Monteiro JM, Griffiths LR, Tucker SJ, Ebers G, Rouleau GA (2010) A dominant-negative mutation in the TRESK potassium channel is linked to familial migraine with aura. Nat Med 16:1157–1160. CrossRef Medline

Lawson SN, Crepps BA, Perl ER (1997) Relationship of substance P to afferent characteristics of dorsal root ganglion neurones in guinea-pig. J Physiol 505:177–191. CrossRef Medline

Lesage F, Reyes R, Fink M, Duprat F, Guillemare E, Lazdunski M (1996) Dimerization of TWIK-1 K^+ channel subunits via a disulfide bridge. EMBO J 15:6400–6407. Medline

Li L, Rutlin M, Abraira VE, Cassidy C, Kus L, Gong S, Jankowski MP, Luo W, Heintz N, Koerber HR, Woodbury CJ, Ginty DD (2011) The functional organization of cutaneous low-threshold mechanosensory neurons. Cell 147:1615–1627. CrossRef Medline

Liu P, Xiao ZM, Ren F, Zhao HC, Cao YQ (2012) The effects of a dominant-negative TRESK/KCNK18 mutation on the excitability of trigeminal ganglion neurons. Society for Neuroscience Abstract.

Marsh B, Acosta C, Djouhri L, Lawson SN (2012) Leak K(+) channel mRNAs in dorsal root ganglia: relation to inflammation and spontaneous pain behaviour. Mol Cell Neurosci 49:375–386. CrossRef Medline

Miller AN, Long SB (2012) Crystal structure of the human two-pore domain potassium channel K2P1. Science 335:432–436. CrossRef Medline

Ophoff RA, Terwindt GM, Vergouwe MN, van Eijk R, Oefner PJ, Hoffman SM, Lamerdin JE, Mohrenweiser HW, Bulman DE, Ferrari M, Haan J, Lindhout D, van Ommen GJ, Hofker MH, Ferrari MD, Frants RR (1996) Familial hemiplegic migraine and episodic ataxia type-2 are caused by

mutations in the Ca^{2+} channel gene CACNL1A4. Cell 87:543–552. CrossRef Medline

Perez-Reyes E (2003) Molecular physiology of low-voltage-activated t-type calcium channels. Physiol Rev 83:117–161. CrossRef Medline

Plant LD (2012) A role for K2P channels in the operation of somatosensory nociceptors. Front Mol Neurosci 5:21. CrossRef Medline

Pumpens P, Grens E (2001) HBV core particles as a carrier for B cell/T cell epitopes. Intervirology 44:98–114. CrossRef Medline

Rahm AK, Gierten J, Kisselbach J, Staudacher I, Staudacher K, Schweizer PA, Becker R, Katus HA, Thomas D (2012) PKC-dependent activation of human K(2P) 18.1 K(+) channels. Br J Pharmacol 166:764–773. CrossRef Medline

Ruan HZ, Moules E, Burnstock G (2004) Changes in P2X3 purinoceptors in sensory ganglia of the mouse during embryonic and postnatal development. Histochem Cell Biol 122:539–551. CrossRef Medline

Sano Y, Inamura K, Miyake A, Mochizuki S, Kitada C, Yokoi H, Nozawa K, Okada H, Matsushime H, Furuichi K (2003) A novel two-pore domain K^+ channel, TRESK, is localized in the spinal cord. J Biol Chem 278:27406–27412. CrossRef Medline

Scherrer G, Imamachi N, Cao YQ, Contet C, Mennicken F, O'Donnell D, Kieffer BL, Basbaum AI (2009) Dissociation of the opioid receptor mechanisms that control mechanical and heat pain. Cell 137:1148–1159. CrossRef Medline

Seal RP, Wang X, Guan Y, Raja SN, Woodbury CJ, Basbaum AI, Edwards RH (2009) Injury-induced mechanical hypersensitivity requires C-low threshold mechanoreceptors. Nature 462:651–655. CrossRef Medline

Snider WD, McMahon SB (1998) Tackling pain at the source: new ideas about nociceptors. Neuron 20:629–632. CrossRef Medline

Staikopoulos V, Sessle BJ, Furness JB, Jennings EA (2007) Localization of P2X2 and P2X3 receptors in rat trigeminal ganglion neurons. Neuroscience 144:208–216. CrossRef Medline

Strassman AM, Raymond SA, Burstein R (1996) Sensitization of meningeal sensory neurons and the origin of headaches. Nature 384:560–564. CrossRef Medline

Stucky CL, Lewin GR (1999) Isolectin B(4)-positive and -negative nociceptors are functionally distinct. J Neurosci 19:6497–6505. Medline

Tao J, Liu P, Xiao Z, Zhao H, Gerber BR, Cao YQ (2012) Effects of familial hemiplegic migraine type 1 mutation T666M on voltage-gated calcium channel activities in trigeminal ganglion neurons. J Neurophysiol 107:1666–1680. CrossRef Medline

Tulleuda A, Cokic B, Callejo G, Saiani B, Serra J, Gasull X (2011) TRESK channel contribution to nociceptive sensory neurons excitability: modulation by nerve injury. Mol Pain 7:30. CrossRef Medline

Victor TW, Hu X, Campbell JC, Buse DC, Lipton RB (2010) Migraine prevalence by age and sex in the United States: a life-span study. Cephalalgia 30:1065–1072. CrossRef Medline

Yan J, Edelmayer RM, Wei X, De Felice M, Porreca F, Dussor G (2011) Dural afferents express acid-sensing ion channels: a role for decreased meningeal pH in migraine headache. Pain 152:106–113. CrossRef Medline

Yoo S, Liu J, Sabbadini M, Au P, Xie GX, Yost CS (2009) Regional expression of the anesthetic-activated potassium channel TRESK in the rat nervous system. Neurosci Lett 465:79–84. CrossRef Medline

Zhou J, Yao SL, Yang CX, Zhong JY, Wang HB, Zhang Y (2012) TRESK gene recombinant adenovirus vector inhibits capsaicin-mediated substance P release from cultured rat dorsal root ganglion neurons. Mol Med Rep 5:1049–1052. CrossRef Medline